eLife

Reviewed Preprint
v1 • September 12, 2024
Not revised

Reviewed Preprint
v2 • April 7, 2026
Revised by authors

For correspondence:
chrisdonnelly@pitt.edu

* Authors share equal contributions

Competing interests: A provisional patent has been filed for the CUTS1 biosensor. CJD is an advisor for Korro Bio.

Funding: See page 27

Reviewing editor: Mychael V Lourenco, Universidade Federal do Rio de Janeiro, Brazil

CUTS RNA Biosensor for the Real-Time Detection of TDP-43 Loss-of-Function

Longxin Xie[1,2,3,*], Jessica Merjane[1,3,*], Cristian A Bergmann[1,3,*], Jiazhen Xu[1,3,4], Shruthi Balasubramaniyan[5,9], Bryan Hurtle[1,3,6], Charleen T Chu[4,5,6,7,8], Christopher J Donnelly[1,3,4,6,7,8]

[1]Department of Neurobiology, University of Pittsburgh School of Medicine, Pittsburgh, United States • [2]School of Medicine, Tsinghua University, Beijing, China • [3]LiveLikeLou Center for ALS Research, University of Pittsburgh School of Medicine, Pittsburgh, United States • [4]Interdisciplinary Biomedical Graduate Program Cellular and Molecular Pathology, University of Pittsburgh, Pittsburgh, United States • [5]Department of Pathology, University of Pittsburgh School of Medicine, Pittsburgh, United States • [6]Center for Neuroscience at the University of Pittsburgh, Pittsburgh, United States • [7]Pittsburgh Institute for Neurodegeneration, University of Pittsburgh, Pittsburgh, United States • [8]Center for Protein Conformational Diseases, University of Pittsburgh, Pittsburgh, United States • [9]Department of Human Genetics, University of Pittsburgh School of Public Health, Pittsburgh, United States

eLife Assessment

This **important** study developed a new sensor for TDP-43 activity that is sensitive and robust that should strongly impact the field's ability to monitor whether TDP-43 is functional or not. The evidence, though limited to cell culture, is **compelling** and is the first demonstration that a GFP on/off system can be used to assess genetic TDP-43 mutants as well as loss of soluble TDP-43.

https://doi.org/10.7554/eLife.101216.2.sa3

Abstract

Mounting evidence implicates TDP-43 dysfunction and the accumulation of pathological cryptic exons across multiple neurodegenerative diseases, underscoring the need for accessible tools to detect and quantify TDP-43 loss-of-function (LOF). These tools are crucial for assessing potential disease contributors and exploring therapeutic candidates in TDP-43 proteinopathies. Here, we develop a sensitive and accurate real-time sensor for TDP-43 LOF: the CUTS (CFTR UNC13A TDP-43 Loss-of-Function) system. This system combines UG-rich sequences and previously reported cryptic exons regulated by TDP-43 with a reporter, enabling the tracking of TDP-43 LOF through live microscopy and RNA/protein-based assays. We show that CUTS effectively detects TDP-43 loss of function arising from mislocalization, impaired RNA binding, and pathological aggregation. Our results show the sensitivity and accuracy of the CUTS system in detecting and quantifying TDP-43 LOF, opening avenues to explore unknown TDP-43 interactions that regulate its function. In addition, by replacing the fluorescent tag in the CUTS system with the coding sequence for TDP-43, we show significant recovery of its function under TDP-43 LOF conditions, highlighting the potential utility of CUTS for self-regulating gene therapy applications. In summary, CUTS represents a platform for evaluating TDP-43 LOF in real-time and gene-replacement therapies in neurodegenerative diseases associated with TDP-43 dysfunction.

Highlights

- CUTS is a cryptic exon RNA biosensor enabling real-time detection of TDP-43 loss of splicing function.
- CUTS exhibits a linear relationship with a reduction in TDP-43 protein.
- CUTS can deliver an autoregulated gene payload in response to TDP-43 loss-of-function.
- TDP-43 homotypic phase transitions and cell stress induce loss of splicing function detected

via CUTS.

Introduction

Amyotrophic lateral sclerosis (ALS) is a progressive and fatal neurodegenerative disease (NND) characterized by a persistent degeneration of the neurons of the spinal cord and motor cortex (Feldman et al., 2022). The dysregulation of the RNA binding protein (RBP), TAR DNA-binding protein 43 (TDP-43) is a hallmark pathobiology observed in ~97% of all ALS patients (Neumann et al., 2006), ~45% of Frontotemporal lobar degeneration (FTLD) patients (Ling et al., 2013; Neumann et al., 2006), and 40%-60% of Limbic Associated TDP-43 Encephalopathy (LATE) patients (McKee et al., 2010; Nelson et al., 2019; Tremblay et al., 2011). Under physiological conditions, TDP-43 orchestrates many cellular processes critical for neuronal health and homeostasis, including regulating RNA metabolism, splicing, and stress response pathways. However, in disease, TDP-43 is depleted from the nucleus and mislocalizes to the cytoplasmic compartment, losing the ability to perform its canonical splicing function and may transition into insoluble aggregates (Hurtle et al., 2023; Mann and Donnelly, 2021).

Recent efforts increasingly focus on the implications of TDP-43's loss of splicing function and its consequence on disease onset and progression (Brown et al., 2022; Buratti and Baralle, 2001; Klim et al., 2019; Ling et al., 2015; Ma et al., 2022; Melamed et al., 2019). Physiologically, TDP-43 selectively binds to specific UG-rich sequences within pre-mRNA transcripts, providing precise control over the alternative splicing of a subset of conserved targets, thereby modulating their gene expression and cellular function (Kuo et al., 2009; Lukavsky et al., 2013). This regulatory function is key in repressing the incorporation of TDP-43-mediated aberrant 'cryptic exons' (CE), non-conserved intronic regions whose inclusion has been linked to cellular toxicity and pathological consequences (Brown et al., 2022; Klim et al., 2019; Ling et al., 2015; Ma et al., 2022; Mehta et al., 2023; Melamed et al., 2019; Polymenidou et al., 2011). Noteworthy examples of transcripts susceptible to aberrant CEs in the absence of functional TDP-43 include *STMN2* (Klim et al., 2019; Melamed et al., 2019) and *UNC13A* (Brown et al., 2022; Ma et al., 2022), both pivotal in maintaining the integrity and physiological function of neurons, such as axon regeneration and motor neuron firing (Shin et al., 2014, 2012; Varoqueaux et al., 2002; Willemse et al., 2023). Therefore, their aberrant splicing patterns and loss-of-function (LOF) in disease highlights the critical role of TDP-43 in preserving neuronal health and function through the regulation of key neuronal health.

A well-established and currently available method to accurately monitor and quantify TDP-43's splicing function has frequently relied on employing cryptic exon 9 inclusion in the human cystic fibrosis transmembrane conductance regulator (CFTR) transgene (Buratti and Baralle, 2001; Ayala et al. 2006). However, this approach can only be used at the RNA level, limiting its functionality as a reporting system for high-throughput screens or *in vivo* applications. Furthermore, endogenous cryptic exons exhibit variable responses to TDP-43 loss, may be cell type-specific, and are still being defined. To address this, we designed a screening tool, the 'CFTR-UNC13A TDP-43 loss-of-function Sensor' (CUTS) system, engineered to detect TDP-43 LOF and output a proportional and quantifiable signal using GFP or other reporters. By combining previously described TDP-43 binding targets with small UG stretches, we significantly improved the sensitivity measurable in real time using standard assays. Functional TDP-43 promotes the splicing of CUTS CE, resulting in a frameshift and early stop codon that prevents GFP expression. TDP-43 LOF activates the CUTS biosensor by promoting the inclusion of the CE, allowing GFP to be expressed. Here, we highlight the CUTS system sensitivity in response to TDP-43 loss. The CUTS design enables GFP expression to be directly proportional to TDP-43 LOF, allowing the detection of changes in TDP-43 function even when alterations cannot be measured directly by traditional methods like qPCR, western blot, or immunofluorescent imaging.

In this study, we highlight the utility and sensitivity of the CUTS biosensor in non-neuronal and neuronal cells. We also show that aberrant TDP-43 phase transitions or mislocalization disrupt TDP-43 splicing function by expressing well-established RNA-binding-deficient and cytoplasmic TDP-43 constructs. We also replaced the GFP cassette in the CUTS biosensor with the wild-type

TARDBP coding sequence (CUTS-TDP43), demonstrating that CUTS can regulate a gene payload expression in response to TDP-43 loss-of-function. The CUTS biosensor provides a sensitive and reliable means to dynamically monitor TDP-43 function and can be applied for therapeutic screening, assessment of disease-associated dysfunction, and delivery of genetic payloads in response to TDP-43 loss.

Results

CUTS TDP-43 LOF sensor design utilizing known Cryptic Exons

To improve the detection of TDP-43 LOF, we designed a novel TDP-43 LOF sensor (TS) using previously reported genes known to undergo TDP-43-regulated splicing (*UNC13A* and *CFTR*). The TS cassettes are constructed with a constitutively expressed mCherry, followed by a TDP-43-regulated CE and a GFP linked to a 3x nuclear localization signal (NLS), each separated by a T2A self-cleavage sequence (Figure 1A). We positioned the GFP reporter outside the mCherry open reading frame (ORF), introducing an early stop codon upstream of the GFP (Figure 1A). This strategic design achieved two key outcomes: (1) Under physiological TDP-43 levels, the binding of TDP-43 to the CE and UG-rich sequence should promote complete intronic splicing, maintaining the in-frame stop codon upstream of GFP, resulting in only mCherry expression. (2) TDP-43 loss and/or failure to bind the CE sites will result in CE retention and a subsequent frameshift that bypasses the stop codon, allowing translation to proceed into the GFP coding sequence, leading to co-expression of mCherry and GFP. This system will allow a systematic screen of whether any TDP-43 perturbation is causing LOF, which should be proportional to GFP signal output.

CUTS is more precise than CFTR and UNC13A as a TDP-43 LOF biosensor

To assess the functionality of TS, we engineered UNC13A-TS, CFTR-TS, and CUTS, which utilized the TDP-43-regulated CEs from UNC13A, CFTR, and a combined construct termed CUTS (CFTR-UNC13A TS), integrating both CE sequences (Figure 1B). Additional base modifications were incorporated into the cassette designs to prevent unexpected stop codons within the CE regions (see Table S1 for full sequence details). Each construct was coupled with a Tet3g promoter, cloned into a Piggybac vector, and stably expressed in HEK293 cells. To evaluate the accuracy and reliability of the three TS constructs, we performed a TDP-43 LOF assay using increasing *siRNA* concentrations, followed by live confocal imaging and western blot (WB) analysis (Figure 1C-G and S1A-H). Across all cell lines, we observed constitutive mCherry expression and a trend toward increased GFP signals with higher *siTDP-43* concentrations. The UNC13A-TS construct demonstrated no detectable GFP expression under control conditions in both imaging-based and WB analyses (Figure 1 C-D, S1A-E). However, the UNC13A-TS showed limited sensitivity, with only a modest GFP signal (17% of CUTS) detected via imaging under the highest dose of siTDP-43 treatment assessed (20nM; Figure 1D). In contrast, the CFTR-TS construct exhibited a notably high baseline, with detectable GFP leakage in control groups without TDP-43 loss (Figure 1C-D, S1A-B, F-H). Interestingly, cells expressing the CUTS construct exhibited a synergistic effect from both the CFTR and UNC13A CE sequences, achieving high sensitivity evidenced by a clear dose-responsive GFP expression with increasing siTDP-43 concentrations, while maintaining high accuracy with minimal leakage via imaging and GFP immunoblotting (Figure 1C-G). Given the promising accuracy of the CUTS sensor, we proceeded to further characterize the CUTS RNA biosensor.

CUTS demonstrates ultra-sensitivity in detecting low-level TDP-43 loss-of-function

To challenge the stability and sensitivity of CUTS, we next conducted an ultra-low dose TDP-43 *siRNA* transfection, ranging from 38-1200 pM. Immunofluorescence staining (IF) revealed a consistent increase in both GFP intensity and GFP-positive cell ratios in CUTS-expressing cells in response to elevated *siTDP-43*, with minimal baseline expression observed (Figure 2A-B). We confirmed the ultra-sensitivity and accuracy of CUTS using WB analysis, demonstrating

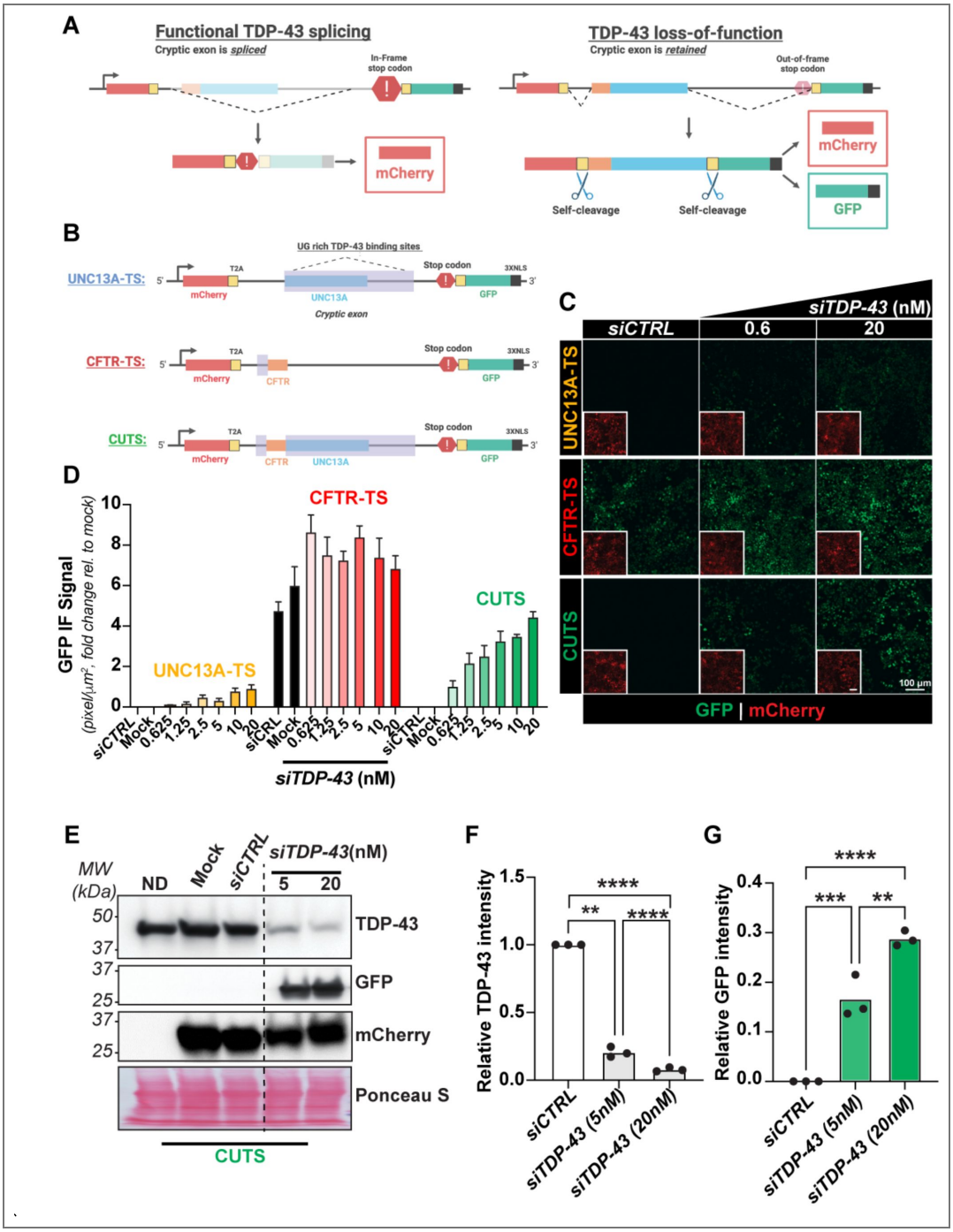

Figure 1. Design and functional comparison of TDP-43 loss-of-function reporter systems.

Comparison of stable polyclonal HEK cells expressing UNC13A-TS, CFTR-TS, or CUTS following treatment with siRNA control (siCTRL) (20nM) or TDP-43 (siTDP-43) (0.6nM - 20nM). Cells were reverse-transfected with siRNA treatment in complete media supplemented with doxycycline (1000 ng/mL). As a negative control, we use ND: No doxycycline. After 72 h, cells were analyzed by live imaging and protein lysate was harvested for western blot analysis. **(A)** Schematic of the TDP-43 loss-of-function Sensor (TS) system design. **(B)** Overview of the UNC13A-TS, CFTR-TS, and CUTS cryptic exon cassette design. **(C)** Representative live imaging of TS comparison (10X) nuclear GFP indicates TDP-43 LOF. **(D)** Mean intensity quantification of GFP signal intensity as shown in (C). **(E)** Western blot analysis of CUTS immunoblotting for TDP-43 and GFP proteins. **(F-G)** Relative pixel quantification of TDP-43 and GFP band normalized to total protein (Ponceau S) from (E). Statistical significance was determined by one-way ANOVA and Tukey's multiple comparison test (*, $p < 0.05$; **, $p < 0.01$; ***, $p < 0.001$; ****, $p < 0.0001$). Green = GFP signal; red = mCherry signal. Scale bar = 100 µm. N=3 biological replicates.

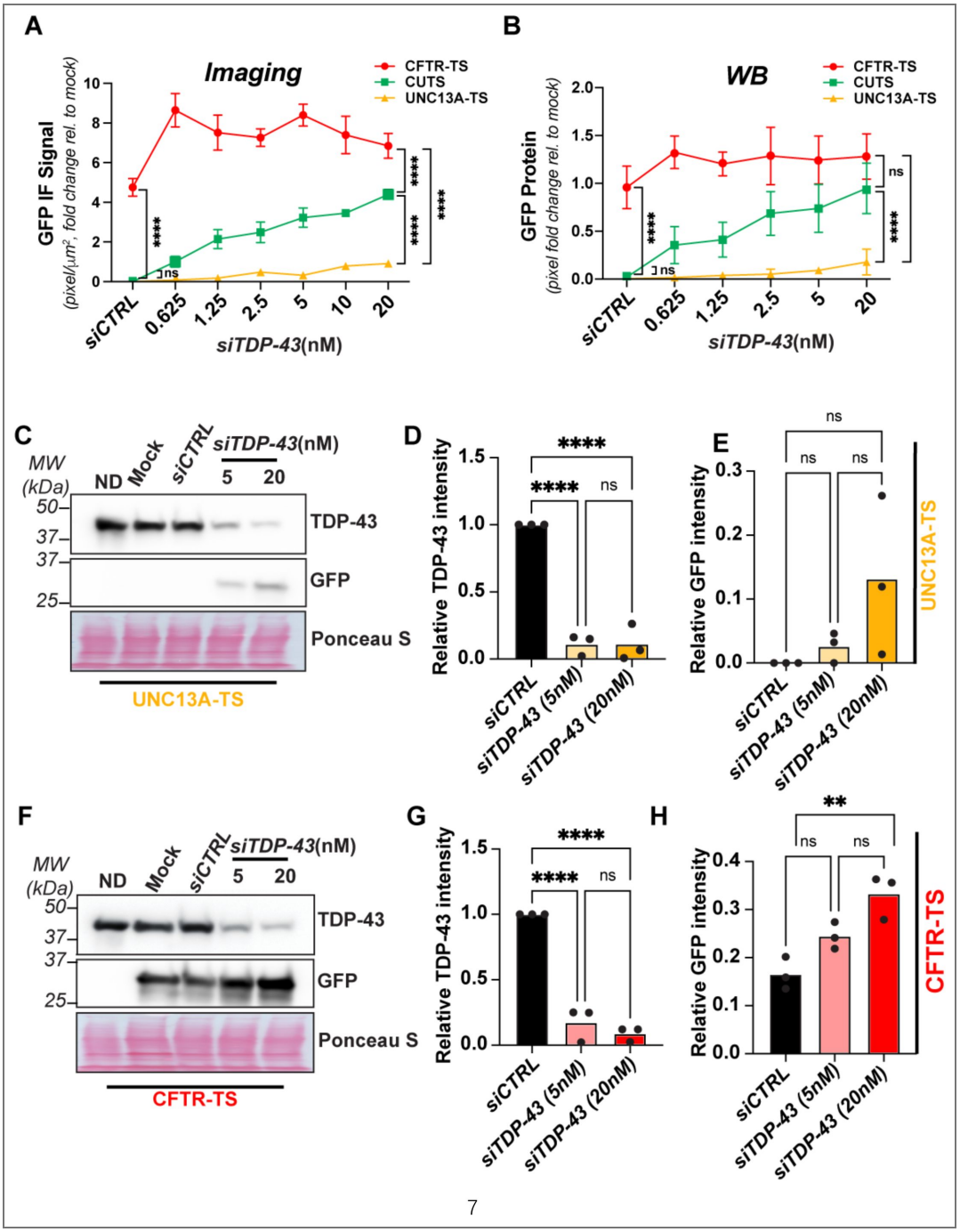

7

Supplementary Figure 1. Differential reporter sensitivity to TDP-43 depletion.

Comparison of stable polyclonal HEK cells expressing UNC13A-TS, CFTR-TS, or CUTS following treatment with siRNA control (siCTRL) (20nM) or TDP-43 (siTDP-43) (0.6nM - 20nM). Cells were reverse-transfected with siRNA treatment in complete media supplemented with doxycycline (1000 ng/mL). After 72 h, cells were analyzed by live imaging and protein lysate was harvested for western blot analysis. (**A)** Mean intensity quantification of GFP signal intensity from live imaging, presented as fold change from mock. **(B)** Relative pixel quantification of GFP normalized to total protein (Ponceau S), presented as fold change from mock. **(C-E)** WB analysis of UNC13A-TS, developing again TDP-43 and GFP proteins, and pixel quantification of TDP-43 and GFP intensity from bands show in (C) normalized to total protein (Ponceau S). **(F-H)** WB analysis of CFTR-TS, developing again TDP-43 and GFP proteins, and pixel quantification of TDP-43 and GFP intensity from bands show in (F) normalized to total protein (Ponceau S). Statistical significance was determined by two-way ANOVA and Tukey's multiple comparison test (*, $p < 0.05$; **, $p < 0.01$; ***, $p < 0.001$; ****, $p < 0.0001$). N=3 biological replicates.

measurable GFP even at the lowest doses of *siTDP-43* assessed (Figure 1C-E). While changes in TDP-43 levels were undetectable by WB at *siTDP-43* doses of 37.5-75 pM (measured as 2% TDP-43 KD by WB, see Figure S2A), the CUTS system demonstrated a 7 to 55-fold increase in GFP expression at these doses compared to baseline (Figure S2A). This increase in GFP expression persisted to the highest siTDP-43 dose (1,200 pM; 98% TDP-43 KD; Figure S2A), resulting in a 118,224-fold increase in GFP compared to baseline. Pearson's correlation analysis confirmed a highly significant relationship between GFP expression and siTDP-43 dose (p=0.0011), while the correlation between measurable TDP-43 and siTDP-43 concentration was less significant (p=0.0429) (Figure 2D-E). Linear regression analysis between the logarithmic GFP fold increase and siRNA doses demonstrated an exceptional linear relationship (R^2=0.9998) (Figure 2E). These results indicate that GFP expression produced by CUTS is a more sensitive method for detecting TDP-43 KD (and therefore LOF) than TDP-43 WB detection. The linear relationship between GFP and siTDP-43 dose also demonstrates the potential of CUTS to be used as a predictive model for TDP-43 LOF.

We assessed CUTS' sensitivity at the transcript level using the *siTDP-43* ultra-low dose curve and RT-qPCR assessment in Figure 2F-I. To determine the relative amount of CUTS' CE retention, we designed primers targeting either the entire transcript or the specific junction sites of the CE (Figure 2F-G). The RT-qPCR quantification demonstrated increased sensitivity at detecting changes in TDP-43 levels compared to WB analysis, with the capability of detecting changes in TDP-43 between each siTDP-43 dose (1 – 70% TDP-43 KD, see Figure 2H and Figure S2B) in a linear manner (R^2 = 0.9303). Using CUTS detection, we observed a clear linear logarithmic relationship between the amount of CUTS CE-retention and the increasing *siTDP-43* doses (R^2=0.9994) (Figure 2I and Figure 2SB). Even at 1% KD in TDP-43, the CUTS system detected a 3-fold increase in CE retention compared to baseline, which increased to a 1,488-fold increase at 70% TDP-43 KD (Figure 2I and Figure 2SB). As with our WB analysis (Figure 2D), there was a significant correlation between GFP expression and TDP-43 and the siTDP-43 dose ($p < 0.0001$ and $p = 0.0279$, respectively). Thus, this data suggests that CUTS is a reliable tool to quantify TDP-43's function across an extensive functional range, highlighting its utility as a TDP-43 LOF biosensor.

Additionally, CUTS demonstrated ultra-sensitivity under low-level TDP-43 KD, beyond the detection limit of both WB and RT-qPCR. We next sought to compare the ultra-sensitive detection capacity of the CUTS sensor with the physiological response of CEs inclusion on genes regulated by TDP-43 (Figure S2E). Using low concentrations of siTDP-43, we were able to recapitulate CUTS sensitivity to detect CE inclusion at low-dose siRNA (75 pM) by RT-PCR. Interestingly, LPR8, ARHGAP32, and ACBD3 CEs displayed a similar pattern, showing progressive CE inclusion with increasing *siTDP-43* doses, starting at 75 pM. However, HDGFL2 showed higher sensitivity to TDP-43 LOF, with detectable exon inclusion even at 38 pM (Figure 2SE). Together, these results establish CUTS as a relevant tool to evaluate sensitively and quantitatively minimal reductions in TDP-43 levels and accurately report its LOF.

Pathological TDP-43 phase transitions or mislocalization activate the CUTS biosensor

In ALS/FTLD, the absolute TDP-43 level remains largely unaffected. Instead, TDP-43 undergoes pathological mislocalization and/or phase transitions likely due to a reduction in RNA binding, which reduces the functional cellular TDP-43. To evaluate whether these events contribute to TDP-43 LOF, we tested CUTS's ability to detect TDP-43 LOF caused by TDP-43 mislocalization or aggregation via aberrant phase transitions. We transfected CUTS HEK293 cells with four tagged TDP-43 isoforms: (1) TDP-43^{WT}, (2) TDP-43^{cyto}, (3) TDP-43^{5FL}, and (4) TDP-43$^{cyto\ 5FL}$. The TDP-43^{cyto} variants contain point mutations located within the nuclear localization signal (NLS) of TDP-43, resulting in cytoplasmic mislocalization (Mann et al., 2019). The 5FL form contains five phenylalanine-to-leucine mutations within the two RNA recognition motif (RRM) domains of TDP-43 that greatly impaired TDP-43's RNA binding ability and were previously reported to form aggregated "anisomes" inside the nucleus (Cohen et al., 2015; Elden et al., 2010; Mann et al.,

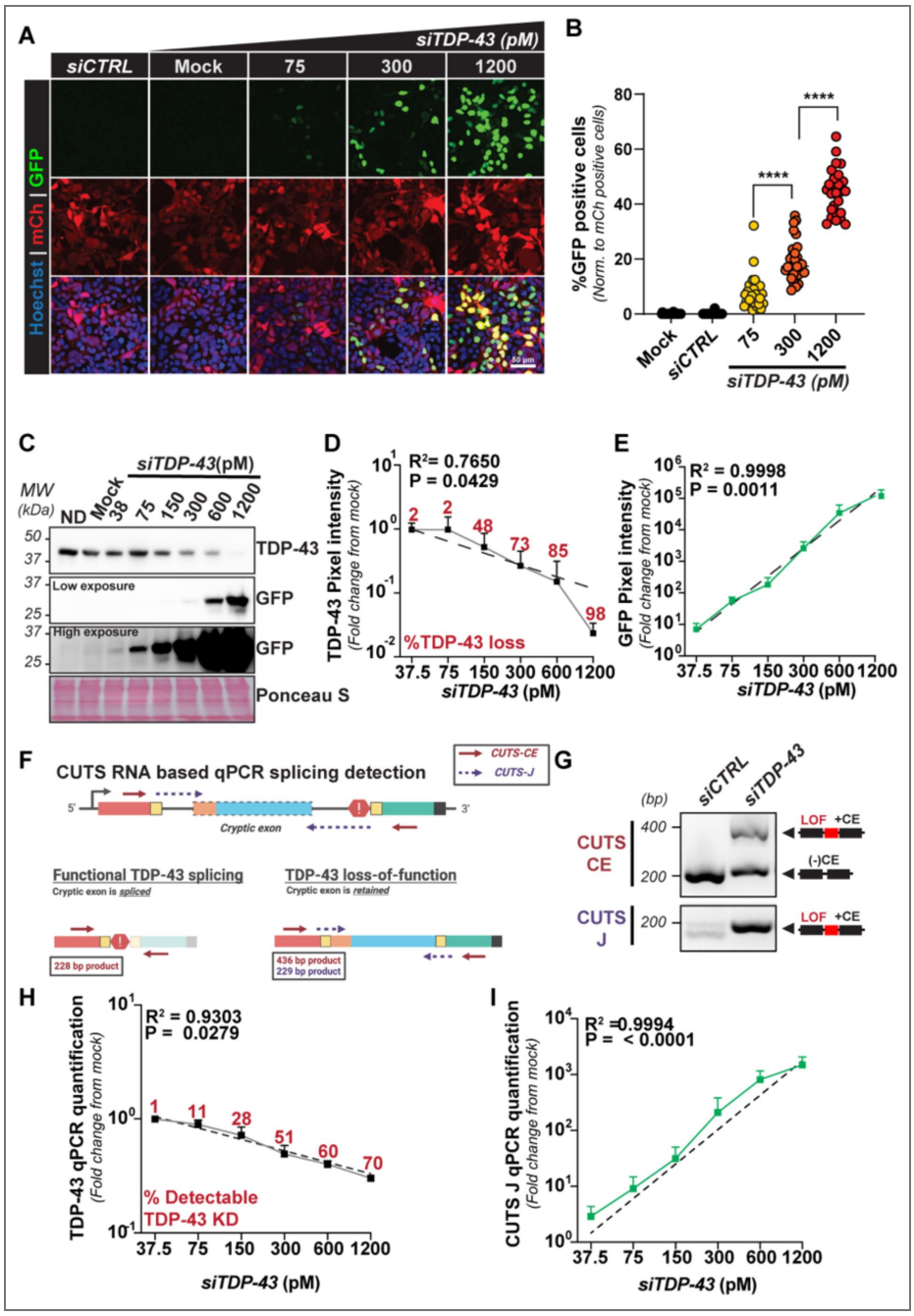

Figure 2. CUTS exhibits linear, dose-responsive activation following low-level TDP-43 knockdown.

Low-dose siRNA TDP-43 (siTDP-43) treatment was performed in stable polyclonal HEK cells expressing CUTS. CUTS-expressing cells were reverse transfected with siRNA control (siCTRL) or siTDP-43 in a dose-response curve (38 to 1200pM) in doxycycline supplemented media (1000ng/ml) for 72hr. **(A)** Representative immunofluorescence images of CUTS-expressing HEK cells under low doses of siRNA TDP-43 treatment. (60X). **(B)** Percentage of GFP-positive cells normalized to the number of CUTS-expressing mCherry-positive cells. **(C)** Western blot of TDP-43 and GFP proteins from HEK cell lysate expressing CUTS under low doses of siRNA TDP-43. Ponceau S is shown as a loading control. **(D)** Pixel intensity quantification of the TDP-43 and **(E)** GFP bands shown in (C), presented as fold-change from the mock-treated sample. **(F)** Schematic showing the position of qPCR primers, developed to detect CUTS cryptic exon inclusion (referred to as 'CUTS-CE' and 'CUTS-J'). **(G)** Representative agarose gel showing qPCR product from melting curve detecting CUTS cryptic exon inclusion using the primers shown in (F). **(H-I)** qPCR quantification of TDP-43 and CUTS cryptic exon J from the siTDP-43 dose curve presented as fold-change from the mock-treated sample. Linear regression analysis shown in (D), (E), (H) and (I) was performed on Log values. Fitting method = least squares regression. (****, $p < 0.0001$). N=3 biological replicates. Green = GFP; red = mCherry. Scale bar = 50 µm. N=3 biological replicates.

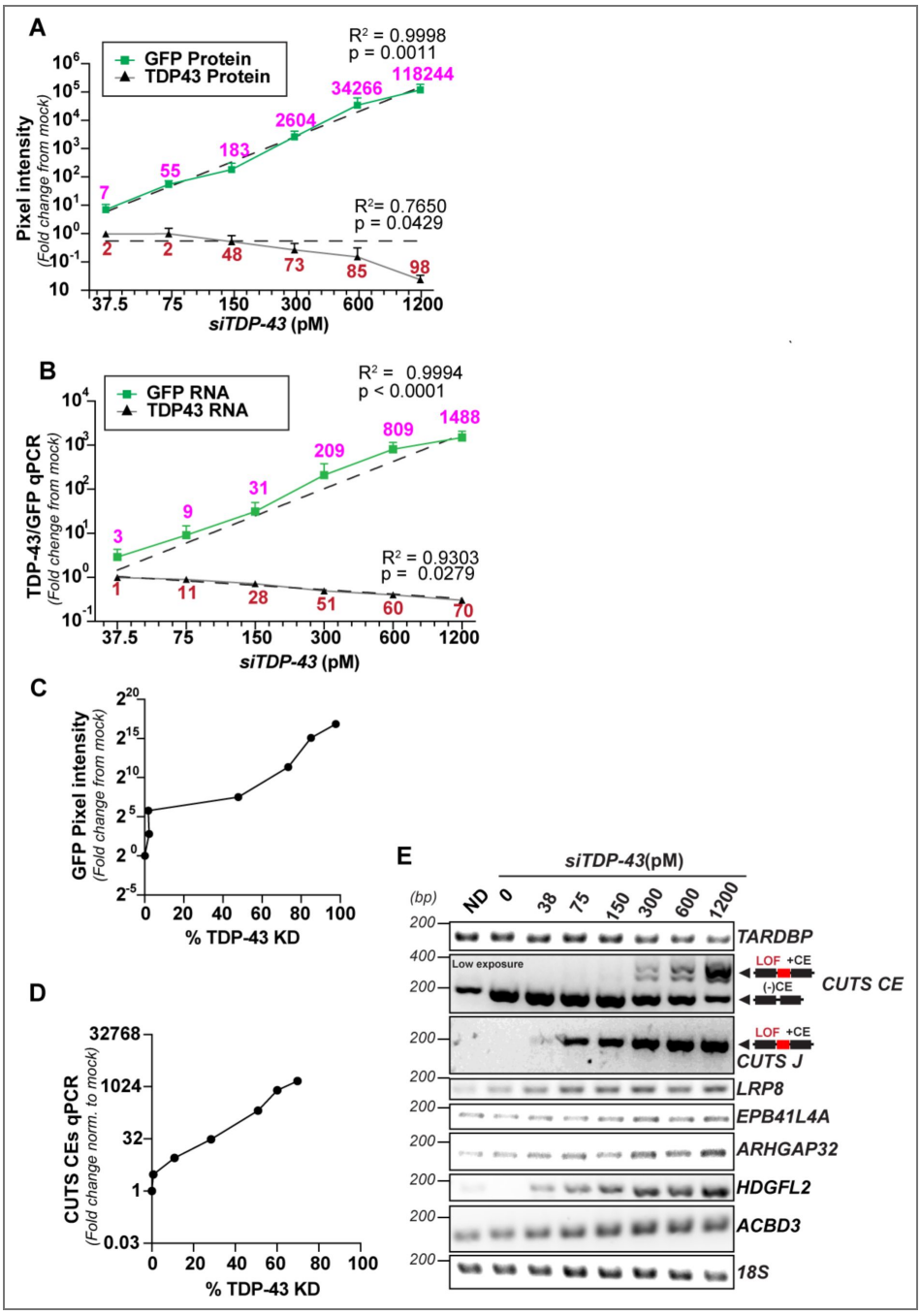

Supplementary Figure 2. CUTS signal scales with dose-dependent TDP-43 knockdown.

Low-dose siTDP-43 treatment was performed in stable polyclonal HEK cells expressing CUTS. CUTS-expressing cells were reverse transfected with siCTRL or siTDP43 in a dose-response curve (38 - 1200 pM) in doxycycline supplemented media (1000ng/ml) for 72 h. **(A)** Pixel intensity quantification of the GFP and TDP-43 bands shown in (C), presented as fold-change from the mock-treated sample. **(B)** qPCR quantification of the siTDP-43 dose curve presented as fold-change from the mock-treated sample. Purple text above indicates the GFP fold change from the mock-treated sample. Red text above indicates the percentage of total detectable TDP-43 knockdown. Linear regression analysis shown in (D) and (G) was performed on Log values. Fitting method = least squares regression. **(C)** GFP pixel intensity from the Western blot shown in Figure 2C plotted against the percentage of TDP-43 knockdown detected under siTDP-43 treatment (38-1200 pM). **(D)** CUTS CE transcript quantification plotted against the percentage of TDP-43 knockdown detected under siTDP-43 treatment (38 - 1200 pM). **(E)** RT-PCR of endogenous cryptic exons and the CUTS biosensor following increasing doses of siTDP43 treatment.

2019; Yu et al., 2021). The TDP-43$^{cyto\ 5FL}$ combines both modifications, leading to insoluble cytoplasmic inclusions (Elden et al., 2010; Keating et al., 2023; Lu et al., 2022; Mann et al., 2019; Yu et al., 2021). Excluding TDP-43^{WT}, all three modified versions have been proven to sequestrate endogenous TDP-43 into mislocalized or aggregated inclusions (Keating et al., 2023). Therefore, our objective was to utilize CUTS to determine whether the expression of these aggregation-prone TDP-43 variants elicits endogenous TDP-43 LOF.

The introduction of TDP-43^{cyto}, TDP-43^{5FL}, and TDP-43$^{cyto\ 5FL}$ induced nuclear GFP signal when assessed by immunofluorescence analysis, while neither the tagged plasmid backbone nor TDP-43^{WT} caused any detectable GFP (Figure 3A). We confirmed the expression of exogenous and endogenous TDP-43 levels by WB and quantified the relative GFP level in each condition (Figure 3B-3C). As we have previously shown that CUTS demonstrates a proportional response to TDP-43's LOF (Figure 2), we were able to directly interpret the relative ability of the different TDP-43 mutants to trigger TDP-43 LOF by comparison of their GFP levels. All three TDP-43 mutants' expression triggered significant LOF compared to the control conditions, albeit at varying significance levels. The most modest LOF effect was achieved by TDP-43^{cyto}, followed by TDP-43$^{cyto\ 5FL}$, and TDP-43^{5FL} (Figure 3C). Interestingly, although both TDP-43^{5FL} and TDP-43$^{cyto\ 5FL}$ caused significantly elevated LOF, the TDP-43^{5FL} mutant alone mediated greater LOF than when combined with the NLS mutations highlighting the potential role of nuclear homotypic TDP-43 interactions potentially contributing to TDP-43 LOF in disease absent its cytoplasmic mislocalization. To further validate the functionality of exogenous TDP-43, we transfected TDP-43^{WT} into a HeLa TDP-43 knock-out cell line expressing CUTS (Roczniak-Ferguson & Ferguson, 2019). We detected a significantly decreased GFP signal compared to the backbone or non-transfected controls, which confirmed the full splicing function of TDP-43^{WT} (Figure S3A-S3D).

We next tested whether CUTS can detect TDP-43 LOF under oxidative stress induced by sodium arsenite ($NaAsO_2$), previously shown to disrupt TDP-43 splicing activity (Huang et al., 2024). CUTS showed mild activation, with detectable GFP signal and a significant increase in GFP intensity compared to mock treated cells (Figure 3D–E). While TDP-43 mRNA levels remained unchanged (Figure 3F), CUTS transcripts were markedly upregulated (Figure 3G). Consistent with this, endogenous cryptic exons ATG4B and GPSM2 were increased, whereas KCNQ2 was unaffected (Figure 3H-I)(Estades Ayuso et al., 2023; Joseph et al., 2025; Schmidt et al., 2019). These results highlight the sensitivity of CUTS in detecting subtle TDP-43 functional loss, which is often difficult to capture using an endogenous marker. Taken together, these data show the functional consequence caused by TDP-43's mislocalization and/or aberrant phase transitions, demonstrating that aggregation-prone TDP-43 variants mediated direct LOF toxicity in addition to any gain-of-function (GOF) toxic events. Furthermore, these results strongly support CUTS's ability to measure functional TDP-43 levels under cell stress and other paradigms beyond TDP-43 KD.

CUTS-mediated autoregulated restoration of TDP-43 splicing

Given the growing recognition of the role TDP-43 LOF is believed to play in disease progression, numerous efforts have been committed to developing rescue methods aimed at re-delivering TDP-43 or other gene payloads to restore its physiological splicing function (Baughn et al., 2023; Mehta et al., 2023; Sun et al., 2017). However, a significant challenge in LOF therapies lies in maintaining precise TDP-43 levels within neurons, as even slight overexpression can lead to GOF toxicity (Johnson et al., 2009; Park et al., 2017; Yang et al., 2022). Consequently, a generalized TDP-43 gene-replacement therapy without genome integration carries a substantial risk of overexpression toxicity. Therefore, a CE biosensor such as CUTS may be used to control cell- and temporal-specific regulation of a gene payload. To test this, we generated a CUTS-controlled TDP-43 (CUTS-TDP43) transgene (Figure 4A). Considering the ultra-sensitivity to TDP-43 LOF and minimal leakage under physiological TDP-43 levels, CUTS-TDP43 may have the potential to autonomously negatively regulate its expression, ensuring levels will not surpass physiological levels.

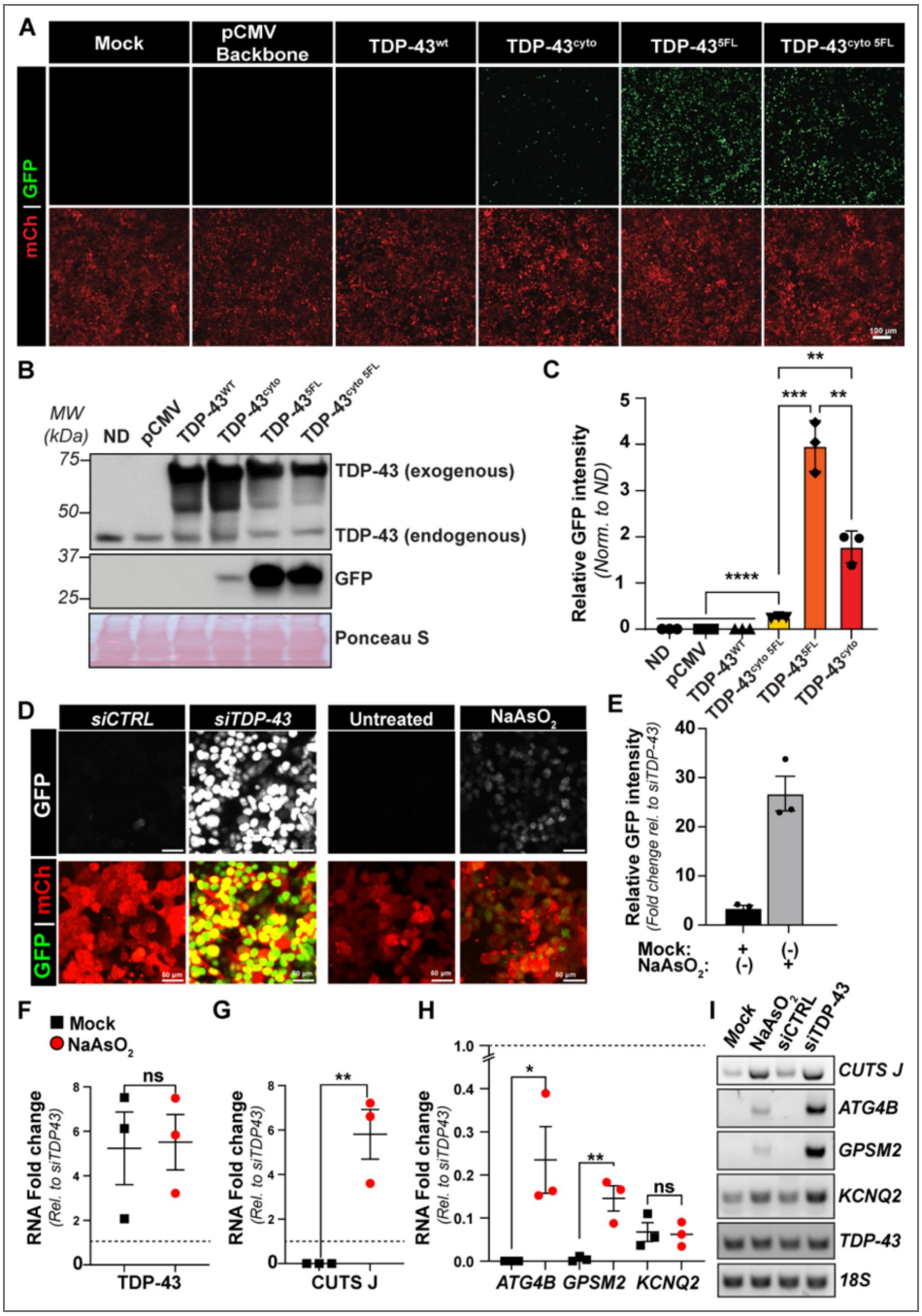

Figure 3. Mislocalization and aberrant phase transitions induce TDP-43 LOF.

Stable HEK cells expressing CUTS were induced with doxycycline (1000 ng/mL) for 24 hours before transfection with the following plasmids: pCMV backbone, TDP-43^{WT}, TDP-43$^{\Delta NLS}$, TDP-43^{5FL}, TDP-43$^{\Delta NLS\ 5FL}$, or non-transfected. Following transfection, plasmids were expressed for 72 h, followed by live imaging and protein analysis. **(A)** Live-imaging of CUTS HEK cells expressing WT or mutant TDP-43 gene cassettes. **(B)** Representative western blot of exogenous and endogenous GFP and TDP-43. Ponceau S is shown as a loading control. **(C)** Relative GFP pixel intensity quantification of the band is shown in (B). **(D–E)** Immunofluorescence of stable HEK cells expressing CUTS with siCTRL (20 nM), siTDP-43 (20 nM), mock, and $NaAsO_2$ (250 µM). **(E)** Immunofluorescence GFP signal quantification of (D) with 250 µM $NaAsO_2$ treatment relative to siTDP-43 (20 nM). **(F-G)** RT-qPCR from CUTS-expressing HEK cells treated with 250 µM $NaAsO_2$ of TDP-43, CUTS-J transcript, and endogenous cryptic exons (ATGB4, GPSM2, and KCNQ2) relative to siRNA TDP-43 20 nM (dotted line) and normalized to 18S. **(I)** RT-PCR from Figure F-H. Expression values were normalized to 18S rRNA, and fold changes were calculated relative to the siTDP-43 (20 nM) condition. Black squares= Mock: Red circle= $NaAsO_2$. Statistical significance was determined by one-way ANOVA and Tukey's multiple comparison test (*, $p < 0.05$; **. $p < 0.01$; ***. $p < 0.001$; ****, $p < 0.0001$). Green = GFP; red = mCherry. Scale bar = 100 µm. N = 3 biological replicates.

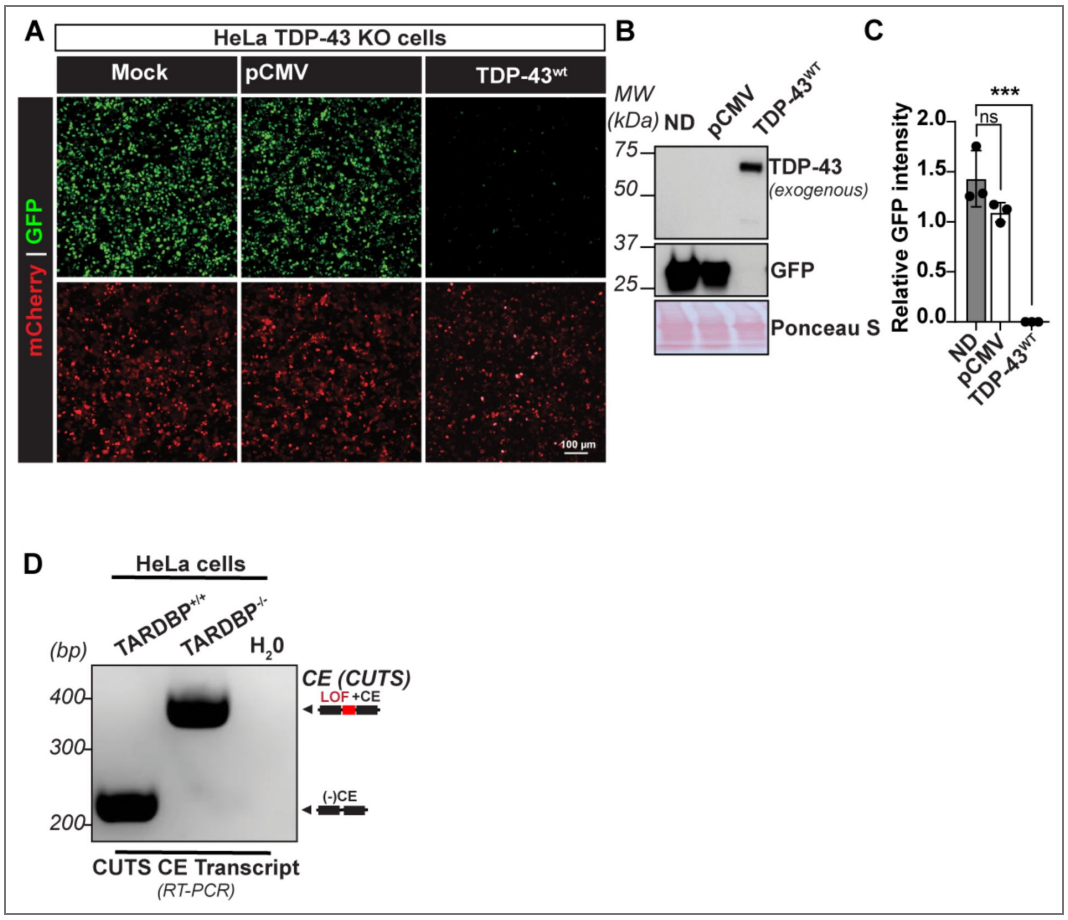

Supplementary Figure 3. TDP-43^{wt} expression rescues loss-of-function in a HeLa TARDBP Knockout Cell Line.

Transient CUTS expression in HeLa TDP-43 KO we induced with doxocycline (1000n/ml) for 24 hours before transfection of pCM backbone or TDP-43^{WT} plasmids. Following transfection, plasmids were expressed for 72 h, followed by live imaging and protein analysis. **(A)** Live-imaging of HeLa TDP-43 KO expressing CUTS in combination with TDP-43^{WT} or pCMV backbone control. **(B)** Representative WB of exogenous and endogenous GFP and TDP-43. Ponceau S is shown as a loading control. **(C)** Relative GFP pixel intensity quantification of the protein bands shown in (B). (**D**)RT-PCR product from CUTS cryptic exon inclusion from wildtype or TDP-43 KO HeLa cell lines using the CUTS-CE primers shown in Figure 2E. Statistical significance was determined by one-way ANOVA and Tukey's multiple comparison test (*, $p < 0.05$; **, $p < 0.01$; ***, $p < 0.001$; ****, $p < 0.0001$). Green = GFP; red = mCherry. Scale bar = 100 µm. N = 3 biological replicates.

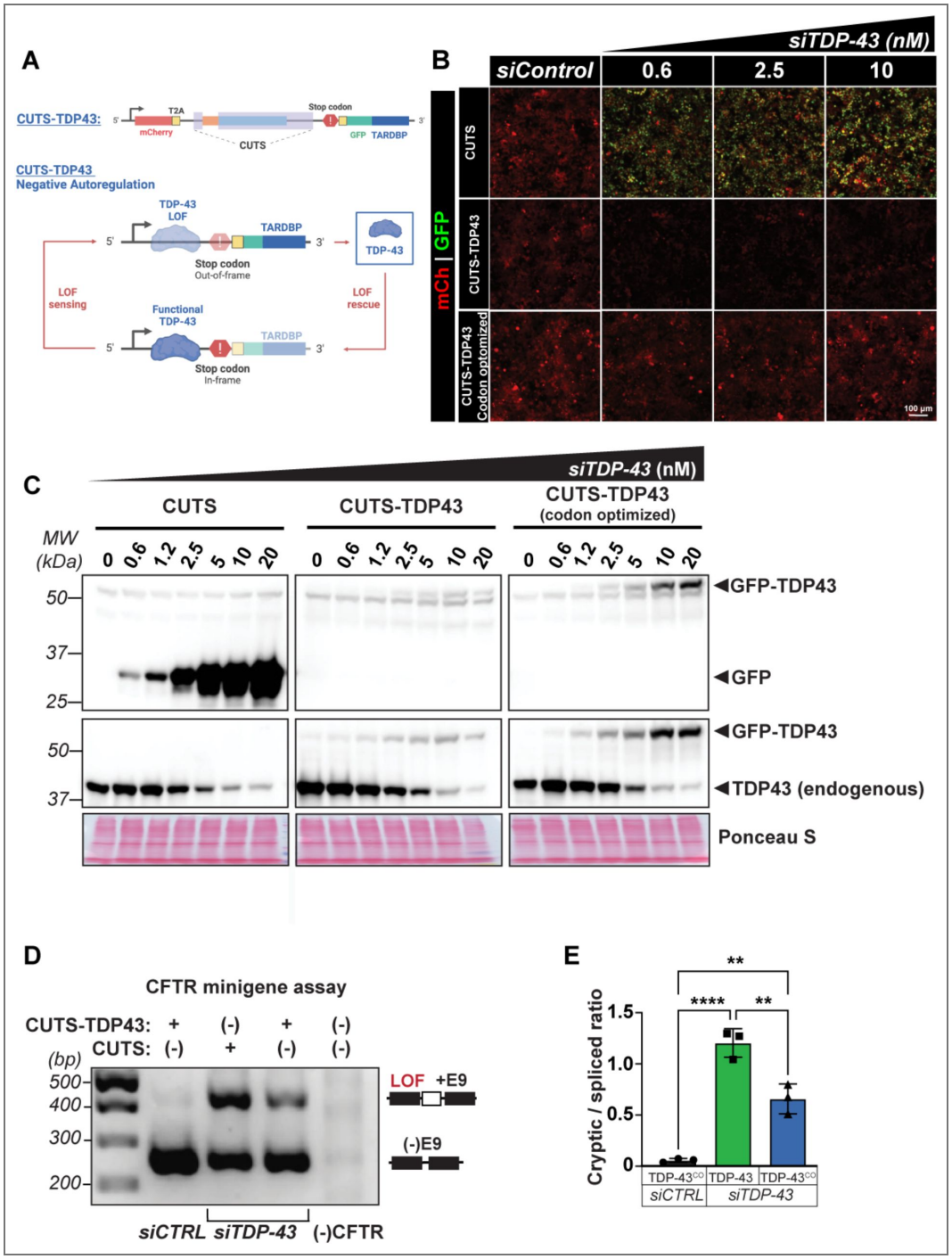

Figure 4. CUTS functions as an autoregulatory controller of TDP-43 expression.

(A) Schematic of CUTS as an autoregulatory controller of TDP-43 expression (CUTS-TDP43). **(B-C)** TDP-43 siRNA (siTDP-43) dose-response curve in stable polyclonal HEK cells expressing CUTS, CUTS-TDP43, or CUTS-TDP-43^{CO} (codon optimized). The codon-optimized variation allows for continued expression during siTDP-43 treatment. HEK cells expressing the CUTS, CUTS-TDP-43 and CUTS-TDP-43^{CO} were reverse transfected with control siRNA (siCTRL) or siTDP-43 in a dose-response curve (0.6nM-20nM) in a doxycycline (1000ng/ml) supplement media for 72hr. Cells were then used for live imaging or protein analysis. (B) Live imaging of the CUTS variants. (C) Immunoblot assay of GFP and TDP-43. Ponceau S is shown as a loading control. **(D-E)** CFTR minigene assay in stable CUTS or CUTS-TDP-43^{CO} expressing HEK cells. Cells were induced with doxycycline (1000 ng/mL) for 24 h before transfection with the CFTR minigene. Following an additional 24h of expression, cells were transfected with 20nM siCTRL or siTDP-43. Cells were harvested 48 h following siRNA transfection for RNA extraction and RT-PCR analysis. (D) PCR agarose gel of CFTR minigene. (E) PCR analysis of the ratio between the CFTR cryptic exon inclusion and the correctly spliced product from CFTR as shown in (D). Statistical significance was determined by One-Way ANOVA and Tukey Post-hoc (**, $p < 0.01$; ****, $p < 0.0001$). Green = GFP; red = mCherry. Scale bar = 100 µm. N=3 biological replicates.

To test this, we created a new polyclonal stable line in HEK293 cells (CUTS-TDP43) by replacing the 3xNLS in the original CUTS cassette with the *TARDBP* ORF fused to a GFP reporter (Figure 4A). However, as our siTDP-43 targets the sequence within the coding region, CUTS-TDP43 was also knocked down upon siRNA transfection, shown by a generalized decreased mCherry signal (Figure 4B). Therefore, we designed a codon-optimized CUTS-TDP43^{CO} that is not targeted by siTDP-43 (Figure 4B). Live imaging analyses showed that CUTS GFP signal demonstrated a steady increase in expression in response to increasing doses of siTDP-43; however, the GFP signal from CUTS-TDP43^{CO} remained undetectable (Figure 4B). WB analysis further demonstrated successful TDP-43 rescue under endogenous TDP-43 KD, as shown by the increasing exogenous TDP-43 observed following decreases in endogenous TDP-43 (Figure 4C). The amount of total TDP-43 appeared to remain consistent throughout the increasing siTDP-43 doses, indicating tight regulation of the rescue parameters. To further confirm whether CUTS-TDP43^{CO} could rescue TDP-43 splicing functionality, we performed a *CFTR* minigene assay (Ayala et al., 2006; Buratti and Baralle, 2001). The expression of CUTS-TDP43^{SO} demonstrated partial, yet significant rescue of cryptic exon 9 splicing in *CFTR* minigene, supporting its controlled efficacy in rescuing splicing LOF (Figure 4D-4E). Taken together, these data indicate that CUTS can autoregulate a TDP-43 payload to physiological levels in response to TDP-43 knockdown.

Modeling CUTS system in neurons

TDP-43 pathology primarily affects neurons; therefore, we adapted the CUTS system for use in human neuronal models. In the original design, CUTS expression was driven by a Tet-On 3G element under the control of the human phosphoglycerate kinase (hPGK) promoter. While hPGK is generally considered a ubiquitous and stable promoter that drives moderate gene expression and performs well in mitotic cells such as HEK293 and HeLa, several studies have reported reduced activity or silencing of PGK-driven transgenes during neuronal differentiation(Xia et al., 2007). To overcome this limitation, we developed an improved version of CUTS in which the Tet-On 3G element is driven by the human synapsin I (hSYN1) promoter, providing more stable and neuron-specific expression. In this optimized construct, we also replaced mCherry with mScarlet to enhance fluorescence intensity and improve the dynamic range of detection. To test the performance of this updated system, we generated stable human neuroblastoma BE(2)-C cell lines expressing CUTS and examined mScarlett and GFP expression under 50 nM of siTDP-43 treatment in 10-day neuron-differentiated stages (Figure 5A-C). We observed robust and inducible CUTS activation following siTDP-43 treatment in differentiated neurons, as shown by GFP mean intensity in MAP-2 positive cells (Figure 5A-D, S4A). Furthermore, TDP-43 immunostaining demonstrated that cells with reduced TDP-43 protein levels corresponded to GFP-positive cells (Figure 5B).

To validate CUTS performance in another human neuronal model, we generated the CUTS human ReN primary neural cells. Stable CUTS-ReN cell lines were generated using a synapsin-driven Tet3G doxycycline-inducible promoter. CUTS-ReN cells were differentiated for three weeks prior to siTDP-43 treatment with increasing concentrations (25–100nM). Live-cell imaging was performed to monitor mScarlet and GFP signals and revealed nuclear GFP in cells with as little as 25 nM TDP-43 siRNA (Figure S4B). Using 100nM siRNA transfection, immunofluorescence analysis of MAP2 and TDP-43 revealed GFP-positive neurons that concurrently showed reduced nuclear TDP-43 levels (Figure 5D; white dotted lines indicate nuclear GFP). Importantly, these GFP-positive cells were negative for the astrocytic marker GFAP (Figure S4C), confirming neuronal specificity of the CUTS response.

Discussion

We developed and characterized the CUTS system, a novel approach to detect TDP-43 LOF. The CUTS system utilizes TDP-43-dependent CE events to correlate the level of TDP-43 LOF directly with the expression of a GFP reporting gene. By combining the CFTR-TS and UNC13A-TS, our findings demonstrate that the CUTS system provides an optimal balance of sensitivity and accuracy. This was evidenced by the ability of CUTS to detect modest levels of TDP-43 LOF, as

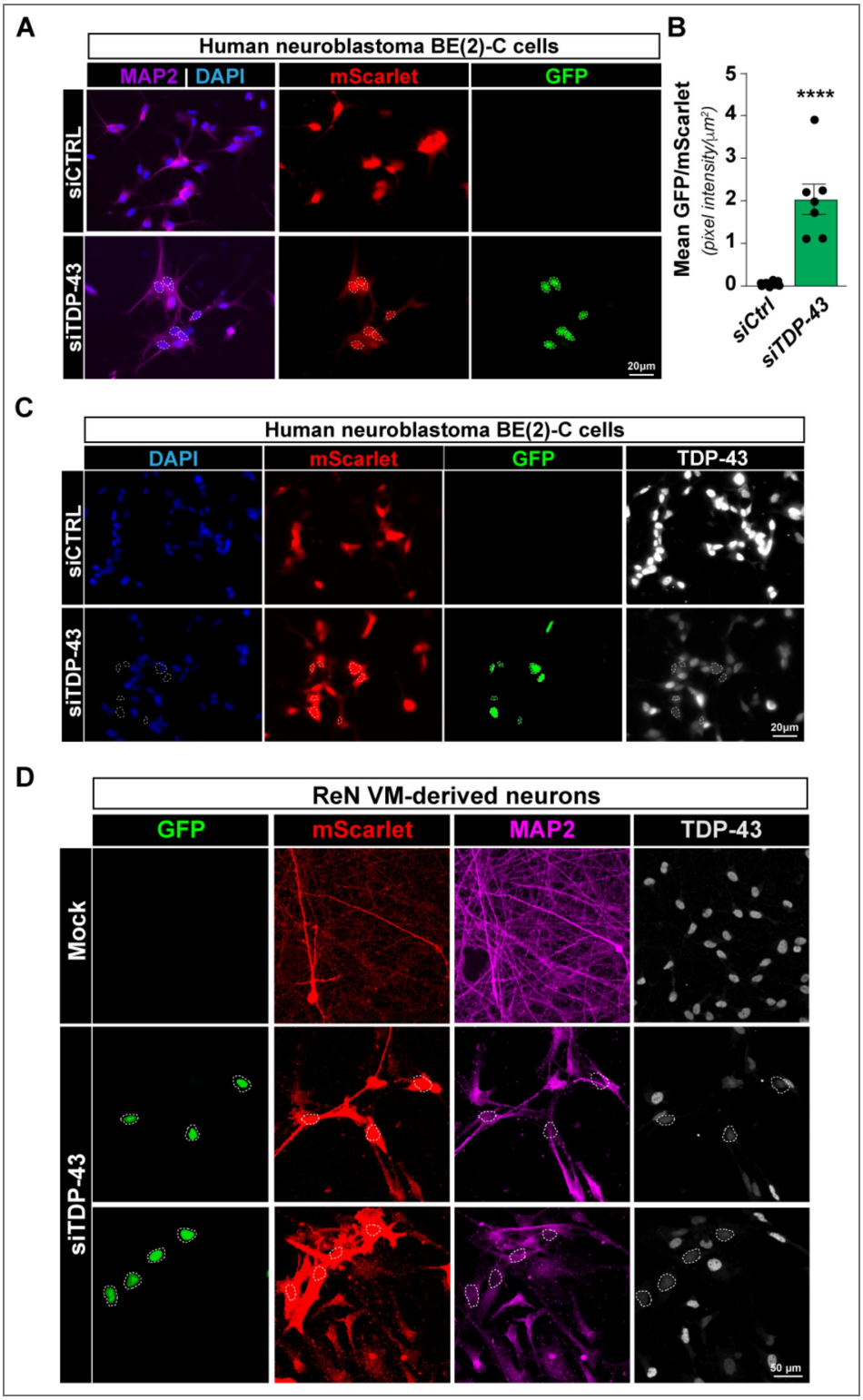

Figure 5. CUTS is activated in human neuronal models in response to TDP-43 LOF.

(A) Representative immunofluorescence images of MAP-2 (magenta), mScarlet, and GFP from CUTS-expressing BE2C neuron-differentiated cells treated with siCtrl or siTDP-43 (50 nM). Scale bar = 20 µM. **(B)** Mean GFP/mScarlet pixel intensity ratios from (A). **(C)** Representative immunofluorescence images of TDP-43 (greyscale) and mScarlet-GFP signal from CUTS-expressing BE(2)-C neuron-differentiated cells show reduced TDP-43 expression following siRNA treatment. Fluorescence intensity quantification shows a 61.9 +/-9.6 percent knockdown. Scalebar = 20 µM. **(D)** Representative immunofluorescence images of MAP-2 (magenta), TDP-43 (grey), mScarlet, and GFP from CUTS-expressing ReN differentiated neurons with 100 nM siRNA TDP-43. Nuclear GFP signals are indicated with a white dotted circle. Scalebar = 50 µM. Non-parametric Kolmogorov-Smirnov T-test (****, $p < 0.0001$).

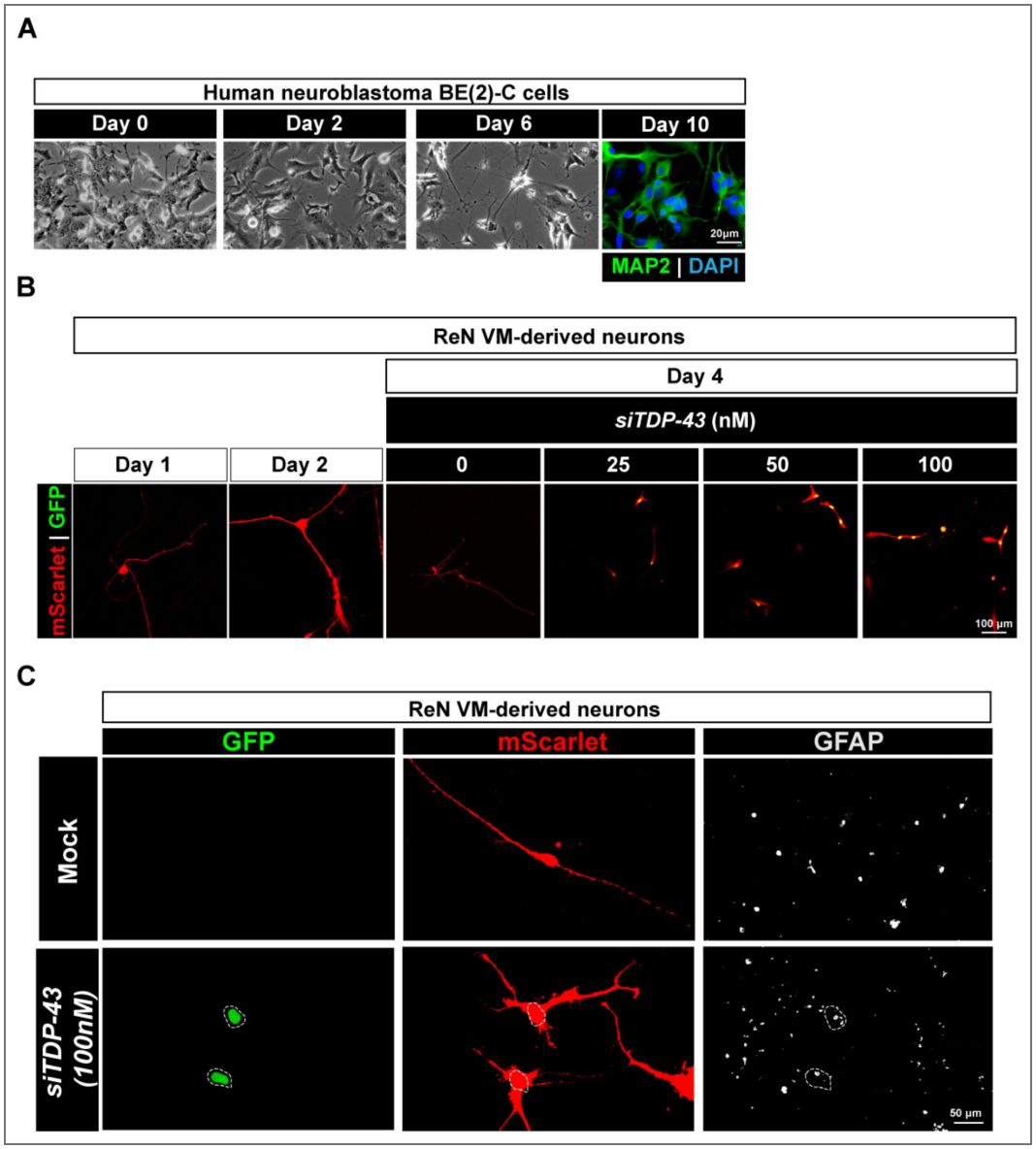

Supplementary Figure 4. CUTS activity in differentiated BE2C and ReN Cells.

(A) Representative bright-field images of BE2C differentiation from day 0 to day 6, after 10 days of differentiation, immunofluorescent staining was performed again MAP-2. Nuclei are indicated with a white dotted circle. Scalebar = 20 mM. **(B)** Representative mScarlet and GFP signal from live imagining of differentiated ReN cells expressing CUTS 2 days before siTDP-43 knockdown and after 96 h of siRNA treatment at different siTDP-43 doses. Scalebar = 100 mM. **(C)** Representative immunofluorescent imaging of CUTS system in differentiated ReN VM cells stained for GFAP (Greyscale). Nuclei are indicated with a white dotted circle. Scalebar = 50 mM.

shown by the dose-responsive increase in the expression of the reporter gene, GFP, under various siTDP-43 concentrations (Figure 2). Furthermore, our results suggest that CUTS can effectively discern TDP-43 LOF induced by pathological phase transitions or mislocalization due to TDP-43 mutant or stressor, a critical aspect in the context of neurodegenerative diseases containing TDP-43 pathology, such as ALS and FTLD. The CUTS system's potential for application in gene-replacement therapies was also highlighted, offering a promising avenue for autoregulated rescue of TDP-43 function, which is critical for avoiding the deleterious effects of TDP-43 overexpression.

This tool findings enables for the significant advancement in the capacity to detect TDP-43 LOF using biosensor assays across diverse experimental settings and through multiple analytical methods. Previously, the *CFTR* minigene assay has been the predominant approach for detecting TDP-43 LOF (Ayala et al., 2006; Buratti and Baralle, 2001; Cohen et al., 2015; Conicella et al., 2020; Jiang et al., 2017; Schmidt et al., 2019). However, this approach is associated with several limitations, all of which are effectively addressed by utilizing the CUTS system. The first advantage of the CUTS system is its ability to detect TDP-43 LOF in real-time through live-imaging analysis. Unlike *CFTR* minigene assays, which typically necessitate endpoint experimental analysis, CUTS facilitates continuous monitoring, eliminating the need for multiple fixed time points. Additionally, CUTS can be seamlessly integrated with various analytical methods, including RT-qPCR (at the RNA level), WB analysis (at the protein level), live imaging (for real-time assessment), and immunofluorescence imaging (to correlate with relevant markers). While not evaluated in this study, it is conceivable that CUTS could be adapted for use with flow cytometry-based techniques, leveraging GFP-positive cells as an output for analysis, as previously demonstrated with a *CFTR*-modified sensor.

In addition to the expanded array of analytical methods offered by CUTS compared to *CFTR* minigene assays, we anticipate that the CUTS system will exhibit superior sensitivity and accuracy. This is supported by the comparison of CUTS with the CFTR-TS or UNC13A-TS cassette (Figure 1), underscoring the potential of CUTS to outperform single minigene-based approaches in TDP-43 LOF detection. Recent work characterizing other CE biosensors indicates that CUTS exhibits comparable or, in some assays, enhanced sensitivity (Wilkins et al., 2024). The expression of the GFP reporter in CUTS achieved up to 118,224-fold increase upon TDP-43 knockdown, compared to *ADNP2* (< 5-fold)(Zhang et al., 2024); TDP-REGv1 (<20-fold); and TDP-REGv2 (<300-fold)(Wilkins et al., 2024). We also show that CUTS can detect ultra-low levels of TDP-43 knockdown (increasing > 7-fold), below the WB or RT-qPCR detection limit. Furthermore, CUTS exhibits a robust log-linear relationship to siRNA doses, making it suitable for quantitative purposes.

The CUTS system outperformed traditional Western blot and transcript-based assays by detecting as little as 1-2% TDP-43 knockdown, which was below the threshold of conventional protein detection methods. This ultra-sensitivity aligns with recent evidence showing that even subtle reductions in TDP-43 can disrupt splicing homeostasis and induce cryptic exon inclusion in physiological targets such as *HDGFL2*, *ARHGAP32*, and *ACBD3* (Brown et al., 2022; Ma et al., 2023; Fratta et al., 2018). The linear correlation between siTDP-43 dose and CUTS reporter output underscores its predictive potential for quantifying graded LOF states. Importantly, the observation that *HDGFL2* cryptic exon inclusion occurs at lower TDP-43 depletion levels supports previous reports identifying it as one of the earliest and most sensitive markers of TDP-43 dysfunction (Humphrey et al., 2020; Seddighi et al., 2023). Thus, CUTS represents a robust and scalable platform to detect and model early TDP-43-dependent splicing alterations.

Due to its success using *in vitro* models, we anticipate that CUTS might similarly be used *in vivo* when coupled with disease models. Integrating the CUTS system with *in vitro* or *in vivo* disease models enables the evaluation of the model's fidelity in recapitulating TDP-43 LOF phenotypes. Such assessments are crucial for selecting appropriate models that faithfully replicate the desired study context. Furthermore, coupling the CUTS system with TDP-43 models presents a valuable approach for diverse screening studies. For example, CUTS can be leveraged for high-throughput drug screening and CRISPR screening methodologies. Such approaches hold promise for

uncovering critical insights into cell-specific disease mechanisms, identifying pivotal disease modifiers, and delineating potential therapeutic genetic targets (Aldewachi et al., 2021; Bock et al., 2022).

A significant advantage of the CUTS system lies in its capacity to deliver precisely regulated gene therapy for rescuing TDP-43 LOF. This study illustrates this capability by placing a functional TDP-43 transcript downstream of the CUTS regulatory elements. The system's self-regulating ability enhances its safety profile as a gene therapy approach, ensuring gene expression occurs only when necessary and exclusively in cells lacking TDP-43 function. Furthermore, this system can be expanded by substituting the TDP-43 transcript with other genetic modifiers of disease, such as antibodies and PROTACs (Pozzi et al., 2019; Tseng et al., 2023), or genes with established therapeutic potential, including heat shock proteins (HSPs) or heterogeneous nuclear ribonucleoproteins (hnRNPs) (Koike et al., 2023; Lu et al., 2022; Yu et al., 2021). This adaptability holds promise for achieving safe therapeutic outcomes without the need for direct TDP-43 expression.

Methods

Generation of plasmids

The CUTS sequence, plasmid, and map were originally generated in this study. The CFTR-TS, UNC13A-TS, CUTS, DNA sequences were designed *in silico* and *de novo* synthesized by Genewiz. These sequences were assembled into Tet3G vector between EcoRI and NotI with NEBuilder HiFi DNA Assembly Master Mix (NEB, E2621L) following the manufacturer's protocol. For CUTS:hSNY1 construction hSYN1 promoter and mScarlet DNA fragment were generated in GenScript and TRE3G promoter was cut from CUTS plasmid by using ClaI and AfeI. After gel recovery (D4001, ZYMO research) these sequences were assembled into Tet3G vector containing CUTS sequence between PPuMI and XmaI with NEBuilder HiFi DNA Assembly Master Mix (NEB, E2621L) following the manufacturer's protocol. Transform mix to competent cell (C2987H, NEB) for the following ampicillin selection. Recombined plasmid was extracted by QIAprep Spin Miniprep Kit (27104, QIAGEN) and confirmed by whole-plasmid sequencing. The full DNA sequence for CUTS, CFTR-TS, UNC13A-TS and CUTS:hSNY1 can be found in Table S1.

The CFTR minigene assay plasmid (pTB-CFTR-A455E) was a kind gift from Dr. Yuna Ayala. The exogenous TDP-43 plasmids were constructed in a pCMV backbone by linking a 3xFlag-APEX2 protein (Addgene #164622) (Bonet-Ponce et al., 2020) to TDP-43 coding sequences with WT, cyto, 5FL, or cyto 5FL modifications (Mann et al., 2019).

The codon-optimized *TARDBP* coding sequence (Table S1) was synthesized by IDT and assembled downstream of the GFP sequence of CUTS with NEBuilder HiFi DNA Assembly Master Mix.

All the primers were synthesized by IDT. All plasmids were verified using whole-plasmid sequencing via Oxford Nanopore, provided by Plasmidsaurus.

Cell culture and transfection

Human Embryonic Kidney 293 (HEK293) cells (female genotype, acquired from the American Type Culture Collection (ATCC)) and HeLa TDP-43 knock-out (KO) cells (a kind gift from Dr. Shawn M Ferguson) (Roczniak-Ferguson and Ferguson, 2019) were cultivated in Dulbecco's Modified Eagle Medium high glucose, pyruvate (DMEM, Thermo Fisher Scientific, 10-313-039) supplemented with 10% HyClone Bovine Growth Serum (Cytiva HyClon, SH3054103HI) and 1X GlutaMAX (Thermo Fisher Scientific, 10-313-039). Cells were incubated at 37°C in a 5% CO2 atmosphere with high humidity. For transfection assays, cells were plated on collagen-coated coverslips or dishes (50 µg/mL, GIBCO) and transfected with designated DNA quantities using Lipofectamine 3000 (Thermo Scientific, L3000015) following the provider's protocol. BE(2)-C neuroblastoma cells were maintained in DMEM/F12 (Gibco; Dulbecco's Modified Eagle Medium/Nutrient Mixture F-12 with GlutaMAX™) supplemented with 10% FBS and cultured until reaching 80–90% confluence. Neuronal differentiation was induced with 10 µM retinoic acid and 50 ng/mL BDNF for 10 days, as

described previously (Targett et al., 2024). ReN VM cells were maintained in proliferation medium consisting of DMEM/F12, B27 supplement, hEGF (20 ng/mL), bFGF (20 ng/mL), and heparin (2 ng/mL) on Matrigel-coated plates. Once cultures reached ~90% confluence, the medium was replaced with differentiation medium (DMEM/F12, B27, and 2 ng/mL heparin) and cells were differentiated for 3 weeks. Full medium changes were performed every other day during the first week, followed by half-medium changes every 4 days thereafter.

Stable cell line generation via PiggyBac transposition

For stable cell line creation, HEK293 or BE(2)-C neuroblastoma cells were pre-plated on 6-well plates and transfected at approximately 70% confluence with 2.5 µg of PiggyBac plasmids encoding CUTS, CFTR-TS, UNC13A-TS, and CUTS-TDP43 for HEKs cells or CUTS:hSNY1 for BE(2)-C alongside with 0.5 µg of the Super PiggyBac Transposase Expressing plasmid (PB200PA-1) using Lipofectamine 3000, according to the manufacturer's guidelines. A transfection control without transposase was included. Following a 48-hour post-transfection period, cells were selected with puromycin (Sigma, P8833) at 5 µg/mL, with media changes every two days. Selection resulted in control cell death within approximately 5 days, while surviving populations were expanded and maintained in reduced puromycin concentrations (2.5 µg/mL) to establish stable lines. Expression of the transgenes was confirmed by immunofluorescence staining and Western blot analysis. ReN VM neuronal precursor cells were electroporated using the 4D-Nucleofector system (Lonza). Cells were subcultured two days before nucleofection to reach ~80% confluence. At confluence, 7.5×10^5 cells were collected, centrifuged, and resuspended in SF buffer (Lonza) containing 0.4 µg of PiggyBac plasmid encoding a CUTS:hSNY1, which is human synapsin driving the Tet-On 3G transactivator gene to activate CUTS expression upon doxycycline treatment, and 0.1 µg PiggyBac transposase plasmid. Electroporation was performed in 16-well Nucleocuvette strips using the CM-137 program. Following a 48-hour post-transfection period, cells were selected with puromycin (Sigma, P8833) at 1 µg/mL, with media changes every two days. Selected CUTS:hSYN1 ReN VM neuronal polyclonal precursor cells were differentiated for 3 weeks. Expression of the CUTS was confirmed in CUTS:hSNY1 ReN VM neurons by live imaging and immunofluorescent staining following treatment with 1000 ng/ml of Doxycycline for 5 days.

Cellular stressor treatment

Sodium arsenite ($NaAsO_2$) was prepared in fresh culture medium to a final concentration of 250 µM and applied to cells by complete medium exchange. For recovery, cells were washed once with fresh medium and subsequently incubated in recovery medium for 5 hours.

SDS-PAGE and Western blot

For protein analysis, cells were lysed directly on the plate using fresh and pre-chilled Urea-RIPA buffer: 2M fresh urea in 1XRIPA buffer (Boston Bioproducts, BP-115X), supplemented with 1% protease inhibitor cocktail (Sigma, P8340) and sonicated. Protein concentrations were quantified using the Pierce BCA Protein Assay Kit (Thermo Scientific, 23227). Proteins were resolved by SDS-PAGE and transferred to nitrocellulose membranes for WB analysis. Membranes were blocked and probed with primary antibodies: mouse-anti-GFP (Santa Cruz, sc-9996, 1:200), mouse-anti-α-tubulin (Sigma, T5168, 1:1000), rabbit-anti-TDP-43 (Proteintech, 10782-2-AP, 1:2500), and rabbit-anti-mCherry (Cell Signaling, 43590, 1:1000), followed by HRP-conjugated secondary antibodies: donkey-anti-mouse (JacksonImmunoResearch 715035151, 1:5000) or donkey-anti-rabbit (JacksonImmunoResearch 711035152, 1:5000). Detection was achieved using Western Lightning ECL Pro (Revvity, NEL1201001EA) or Supersignal West Femto Maximum Sensitivity Chemiluminescent Substrate (Thermo Scientific, 34095) in an Amersham ImageQuant 800 GxP biomolecular imager system (Amersham, 29653452).

Fluorescence microscopy

Confocal imaging was performed on a Nikon A1 laser-scanning microscope using either a 60X oil immersion or a 10X/20X objective for live-cell observations. A Tokai HIT stage-top incubator maintained the required environmental conditions. Representative images were chosen from at least two independent experiments with a minimum of three biological replicates each. For live imaging quantification, we measured the mean GFP signal intensity for each experimental condition. The values were then averaged, and the results were used to calculate and plot the fold change. For immunofluorescent imaging, we first created maximum intensity projection images. We then applied masks to the GFP, mCherry/mScarlet, and Hoechst signals. By overlapping the GFP and mCherry/mScarlet signals, we identified the number of GFP-positive cells. Similarly, by overlapping the mCherry/mScarlet signal with the Hoechst mask, we identified the CUTS-expressing cells. We then calculated a ratio of GFP-positive cells to CUTS-expressing cells, plotted as a percentage of GFP-positive cells using the Nikon NIS software. Neuron-differentiated BE(2)-C cells were stained for MAP2 (Millipore Cat# A5622, 1:500), TDP-43 (Proteintech, 10782-2-AP, 1:500) and Hoechst (1:10,000) and imaged using an Olympus IX71 inverted microscope equipped with 40X objective, a DP80 camera, and Olympus cellSens software. Fluorescence intensity ratios were calculated across multiple image fields using ImageJ FIJI.

siRNA

All siRNA treatments were performed as described using RNAiMAX (Thermo Scientific, 13778150) per manufacturers protocols. All siRNA experiments in CUTS:hSNY1 ReN VM neurons were performed with RNAiMAX reagent and siRNA 48 h after Doxycycline treatment (1000 ng/ml). Quantification occurred and quantified after 120 hr post RNAi treatment (168 hr post Doxycycline treatment). Reverse transfections of siRNA were conducted using RNAiMAX reagent adhering to the supplier's protocol. To knockdown TDP-43, the following siRNAs were used: ON-TARGETplus SMARTpool siRNA against *TARDBP* (Dharmaco, L-012394-00-0005) and siGENOME non-Targeting siRNA for control (Dharmaco, D-001206-13-05).

RNA extraction, RT-PCR, and qPCR

The RT-PCR or RT-qPCR was conducted with cDNA diluted 10-fold. For RT-PCR assay, CFTR cryptic exon region was amplified with the following primer pair: P690-F (5'-CAACTTCAAGCTCCTAAGCCA CTGCCTGC) and P691-R(5'TAGGATCCGGTCACCAGGAAGTTGGTTAAATCA). CUTS' cryptic exon region was amplified with the following primer pair: CUTS-CE-F (5'-ATCCCGGCCCTGGATCCG) and CUTS-CE-R (5'-GTCAGCTTGCCGTAGGTGGC). Endogenous cryptic exons including *LRP8*, *EPB41L4A*, *ARHGAP32*, *ACBD3* and *HDGFL2* were amplified with the following primer pair: LRP8-CE-F(5'-GGA CGAGTTCCAGTGTGGG) and LRP8-CE-R(5' GAAATCTGCGGGGACCCT); EPB41L4A-CE F (5'AGTCACCTT ACAAAACAGAAGTCACA) and EPB41L4A-CE-R(5'-ACATATGCACACACACTCTCACA); ARHGAP32-CE-F (5'GGAGGAAGCATTTTGGAGGTTTCTA) and ARHGAP32-CE-R (5'-CAGCCAAATGCACAGCGAAT); ACBD3-CE-F (5'-ACAGTATCCAGGGAACTACGAA) and ACBD3-CE-R (5'-GCTTCCAGAGAAAGTACCTGTT GC); HDGFL2-CE-F (5'-AAGACGCCTGCGCTAAAGAT) and HDGFL2-CE-R(5'-GCTTCCCTCCCTTCTGATG C). TDP-43 and 18s were amplified using the following primers *RPS18*_FW (5'-GCAGAATCCACGCCA GTACA) and RPS18_REV (5'-TTC ACGGAGCTTGTTGTCCA); *huTDP-43*_FW (5'-TCATCCCCAAGCCATTCA GG) and REV (5'-TGC TTA GGT TCG GCA TTG GA). PCR products were separated by agarose gel electrophoresis, and the bands were visualized with Amersham ImageQuant 800 GxP biomolecular imager system.

For RT-qPCR assay, SsoAdvanced™ Universal SYBR Green Supermix (Biorad, 1725272) was used following the supplier's protocol on a CFX96 Touch Real-Time PCR Detection System (Biorad). Three technical replicates were included for each sample with the following program: 95°C for 30 s, 40 cycles of 95°C for 15 s and 60°C for 20 s. CUTS-CE-F (5'-ATCCCGGCCCTGGATCCG) and CUTS-CE-R (5'-GTCAGCTTGCCGTAGGTGGC) were used to quantify normal CUTS transcript. CUTS-J-F (5'-TCCG GCGAGGGATTTGGG) and CUTS-J-R (5'-CCCCACCTAGACCCATCTCTCC) were primers targeting the cryptic exon junctions to quantify cryptic exon-specific CUTS transcripts. Relative quantification of CUTS cryptic exon was determined by the ΔCt value of CUTS-J normalized to CUTS-CE.

Statistical analysis

Statistical significance was evaluated using GraphPad Prism 9 software, and specific tests used for each experiment are outlined in the respective figure legends.

Data availability

All data generated or analysed during this study are included in the manuscript and its supplementary source data files. Source data underlying the figures will be provided upon request.

Domains of the sequence	Sequence
1. UNC13A-TS mCherry Linker-T2A HBA1_exon2 HBA1_intron 2 HBA1_exon3 UNC13A_modified_CE UNC13A_intron20 Linker-T2A EGFP 3XNLS	ATGGTGAGCAAGGGCGAGGAGGATAACATGGCCATCATCAAGG AGTTCATGCGCTTCAAGGTGCACATGGAGGGCTCCGTGAACGG CCACGAGTTCGAGATCGAGGGCGAGGGCGAGGGCCGCCCCTA CGAGGGCACCCAGACCGCCAAGCTGAAGGTGACCAAGGGTGG CCCCCTGCCCTTCGCCTGGGACATCCTGTCCCCTCAGTTCATGT ACGGCTCCAAGGCCTACGTGAAGCACCCCGCCGACATCCCCGA CTACTTGAAGCTGTCCTTCCCCGAGGGCTTCAAGTGGGAGCGC GTGATGAACTTCGAGGACGGCGGCGTGGTGACCGTGACCCAGG ACTCCTCCCTGCAGGACGGCGAGTTCATCTACAAGGTGAAGCTG CGCGGCACCAACTTCCCCTCCGACGGCCCCGTAATGCAGAAGA AGACCATGGGCTGGGAGGCCTCCTCCGAGCGGATGTACCCCGA GGACGGCGCCCTGAAGGGCGAGATCAAGCAGAGGCTGAAGCT GAAGGACGGCGGCCACTACGACGCTGAGGTCAAGACCACCTAC AAGGCCAAGAAGCCCGTGCAGCTGCCCGGCGCCTACAACGTCA ACATCAAGTTGGACATCACCTCCCACAACGAGGACTACACCATC GTGGAACAGTACGAACGCGCCGAGGGCCGCCACTCCACCGGC GGCATGGACGAGCTGTACAAGGGAGGTGGGGGATCTGGTGAG GGCAGAGGCAGTCTGCTGACATGCGGTGACGTGGAAGAGAATC CCGGCCCTGGATCCGGCCCGGTCAACTTCAAGGTGAGCGGCGG GCCGGGAGCGATCTGGGTCGAGGGGCGAGATGGCGCCTTCCT CGCAGGGCAGAGGATCACGCGGGTTGCGGGAGGTGTAGCGCA GGCGGCGGCTGCGGGCCTGGGCCCTCGGCCCCACTGACCCTC TTCTCTGCACAGCTCCTAAGCCACTGCCTGCTGGTGACCTCTGC CTGGGTTTCCTGGAAAGAACTCTTATCCCCAGGAACTAGTTTGTT GAATAAATGCTGGTGTGAATGTGAATGGATGATTGAACAGATGA ATGAGTGTGATGAGTATGATAAAAGCATGGATGGAGAGATGGGT GAGTACATGGATGGATAGATGGATGAGTTGGTGGGTAGATTCGT GGCTAGATGGATGATGGATGGATGGATGGATGGATGGATGGAT GGACAGATGGATGGATATATGATTGAACTATTGAAAGTATAGATG TATGGATGGGTGAATTTGGGGGTAATTGTTAGATGATGGATGTG GATGGTTGTGAGTGGCTGGTGGACAGACGAAAAATGGATGGGT GGATAAATTGATGGGTGGATGGATGGTTGGTTGTATGAAAGAAT GAATGATTGGGTAGATAAAAGAGTAGATGAATGAATTAATGAATA AACAGGCAGATGGATGATGTAAGCTGCCCCAGACCCTGGGACC TCTGACCCCCGGCGACCCCTTGCACTCTCCATGAGCCCTTTCCT

	TTTTTTTCCTCAGGTCTAGGTGGGGGATCTGGTGAGGGCAGAGG CAGTCTGCTGACATGCGGTGACGTGGAAGAGAATCCCGGCCCT TCTAGAAGCAAGGGCGAGGAGCTGTTCACCGGGGTGGTGCCCA TCCTGGTCGAGCTGGACGGCGACGTAAACGGCCACAAGTTCAG CGTGTCCGGCGAGGGCGAGGGCGATGCCACCTACGGCAAGCT GACCCTGAAGTTCATCTGCACCACCGGCAAGCTGCCCGTGCCC TGGCCCACCCTCGTGACCACCCTGACCTACGGCGTGCAGTGCT TCAGCCGCTACCCCGACCACATGAAGCAGCACGACTTCTTCAAG TCCGCCATGCCCGAAGGCTACGTCCAGGAGCGCACCATCTTCTT CAAGGACGACGGCAACTACAAGACCCGCGCCGAGGTGAAGTTC GAGGGCGACACCCTGGTGAACCGCATCGAGCTGAAGGGCATCG ACTTCAAGGAGGACGGCAACATCCTGGGGCACAAGCTGGAGTA CAACTACAACAGCCACAACGTCTATATCATGGCCGACAAGCAGA AGAACGGCATCAAGGTGAACTTCAAGATCCGCCACAACATCGAG GACGGCAGCGTGCAGCTCGCCGACCACTACCAGCAGAACACCC CCATCGGCGACGGCCCCGTGCTGCTGCCCGACAACCACTACCT GAGCACCCAGTCCGCCCTGAGCAAAGACCCCAACGAGAAGCGC GATCACATGGTCCTGCTGGAGTTCGTGACCGCCGCCGGGATCA CTCTCGGCATGGACGAGCTGTACAAGCTGCAGAGCAGGGCCGA CCCCAAGAAGAAGAGGAAGGTGGACCCCAAGAAGAAGAGGAAG GTGGACCCCAAGAAGAAGAGGAAGGTGTGA
2. CFTR-TS mCherry Linker-T2A CFTR_intron 8 CFTR_modified_exon9 CFTR_intron 9 Linker-T2A EGFP 3XNLS	ATGGTGAGCAAGGGCGAGGAGGATAACATGGCCATCATCAAGG AGTTCATGCGCTTCAAGGTGCACATGGAGGGCTCCGTGAACGG CCACGAGTTCGAGATCGAGGGCGAGGGCGAGGGCCGCCCCTA CGAGGGCACCCAGACCGCCAAGCTGAAGGTGACCAAGGGTGG CCCCCTGCCCTTCGCCTGGGACATCCTGTCCCCTCAGTTCATGT ACGGCTCCAAGGCCTACGTGAAGCACCCCGCCGACATCCCCGA CTACTTGAAGCTGTCCTTCCCCGAGGGCTTCAAGTGGGAGCGC GTGATGAACTTCGAGGACGGCGGCGTGGTGACCGTGACCCAGG ACTCCTCCCTGCAGGACGGCGAGTTCATCTACAAGGTGAAGCTG CGCGGCACCAACTTCCCCTCCGACGGCCCCGTAATGCAGAAGA AGACCATGGGCTGGGAGGCCTCCTCCGAGCGGATGTACCCCGA GGACGGCGCCCTGAAGGGCGAGATCAAGCAGAGGCTGAAGCT GAAGGACGGCGGCCACTACGACGCTGAGGTCAAGACCACCTAC AAGGCCAAGAAGCCCGTGCAGCTGCCCGGCGCCTACAACGTCA ACATCAAGTTGGACATCACCTCCCACAACGAGGACTACACCATC GTGGAACAGTACGAACGCGCCGAGGGCCGCCACTCCACCGGC GGCATGGACGAGCTGTACAAGGGAGGTGGGGGATCTGGTGAG GGCAGAGGCAGTCTGCTGACATGCGGTGACGTGGAAGAGAATC

	CCGGCCCTGGATCCGGCGAGGTGAGTATGGTACATAAAACAAG CATCTATTGAAAATATCTGACAAACTCATCTTTTATTTTTGATGTG TGTGTGTGTGTGTGTGTGTGTGTTTTTTTTTTAACAGGGATTTGGG GAATTATTTGAGAAAGCAAAACAAAACAATAACAATAGAAAAACT TCTAATGGTGATGACAGCCAAGATAGAAAGAGGACAGTTGTTGG AGGTTGCTGGATCCACTGGAGCAGGCAAGGTAGTTCTTTTGTTC TTCACTATTAAGAACTTAATTTGGTGCCCATGTCTCTTTTTTTTTC TAGTTTGTAGTGCTGGAAGGTATTTTTGGAGAAATTCTTACATGA GCATTAGGAGAATGTATGGGTGTAGTGTCTTGTATAATAGAAATT GTTCCACTGATAATTTACTCTAGTTTTTTATTTCCTCATATTATTTT CAGTGGCTTTTTCTTCCACATCTTTATATTTTGCACCACATTCAAC ACTGTATCTTGCACATGGCGAGCATATGGTCGATGATGTAAGCT GCCCCAGACCCTGGGACCTCTGACCCCCGGCGACCCCTTGCAC TCTCCATGAGCCCTTTCCTTTTTTTTCCTCAGGTCTAGGTGGGGG ATCTGGTGAGGGCAGAGGCAGTCTGCTGACATGCGGTGACGTG GAAGAGAATCCCGGCCCTTCTAGAAGCAAGGGCGAGGAGCTGT TCACCGGGGTGGTGCCCATCCTGGTCGAGCTGGACGGCGACGT AAACGGCCACAAGTTCAGCGTGTCCGGCGAGGGCGAGGGCGAT GCCACCTACGGCAAGCTGACCCTGAAGTTCATCTGCACCACCG GCAAGCTGCCCGTGCCCTGGCCCACCCTCGTGACCACCCTGAC CTACGGCGTGCAGTGCTTCAGCCGCTACCCCGACCACATGAAG CAGCACGACTTCTTCAAGTCCGCCATGCCCGAAGGCTACGTCCA GGAGCGCACCATCTTCTTCAAGGACGACGGCAACTACAAGACCC GCGCCGAGGTGAAGTTCGAGGGCGACACCCTGGTGAACCGCAT CGAGCTGAAGGGCATCGACTTCAAGGAGGACGGCAACATCCTG GGGCACAAGCTGGAGTACAACTACAACAGCCACAACGTCTATAT CATGGCCGACAAGCAGAAGAACGGCATCAAGGTGAACTTCAAGA TCCGCCACAACATCGAGGACGGCAGCGTGCAGCTCGCCGACCA CTACCAGCAGAACACCCCCATCGGCGACGGCCCCGTGCTGCTG CCCGACAACCACTACCTGAGCACCCAGTCCGCCCTGAGCAAAG ACCCCAACGAGAAGCGCGATCACATGGTCCTGCTGGAGTTCGT GACCGCCGCCGGGATCACTCTCGGCATGGACGAGCTGTACAAG CTGCAGAGCAGGGCCGACCCCAAGAAGAAGAGGAAGGTGGACC CCAAGAAGAAGAGGAAGGTGGACCCCAAGAAGAAGAGGAAGGT GTGA
3. CUTS mCherry Linker-T2A	ATGGTGAGCAAGGGCGAGGAGGATAACATGGCCATCATCAAGG AGTTCATGCGCTTCAAGGTGCACATGGAGGGCTCCGTGAACGG CCACGAGTTCGAGATCGAGGGCGAGGGCGAGGGCCGCCCCTA CGAGGGCACCCAGACCGCCAAGCTGAAGGTGACCAAGGGTGG

CFTR_intron 8 CFTR_modified_exon9 UNC13A_modified_CE UNC13A_intron20 Linker-T2A EGFP 3XNLS	CCCCCTGCCCTTCGCCTGGGACATCCTGTCCCCTCAGTTCATGT ACGGCTCCAAGGCCTACGTGAAGCACCCCGCCGACATCCCCGA CTACTTGAAGCTGTCCTTCCCCGAGGGCTTCAAGTGGGAGCGC GTGATGAACTTCGAGGACGGCGGCGTGGTGACCGTGACCCAGG ACTCCTCCCTGCAGGACGGCGAGTTCATCTACAAGGTGAAGCTG CGCGGCACCAACTTCCCCTCCGACGGCCCCGTAATGCAGAAGA AGACCATGGGCTGGGAGGCCTCCTCCGAGCGGATGTACCCCGA GGACGGCGCCCTGAAGGGCGAGATCAAGCAGAGGCTGAAGCT GAAGGACGGCGGCCACTACGACGCTGAGGTCAAGACCACCTAC AAGGCCAAGAAGCCCGTGCAGCTGCCCGGCGCCTACAACGTCA ACATCAAGTTGGACATCACCTCCCACAACGAGGACTACACCATC GTGGAACAGTACGAACGCGCCGAGGGCCGCCACTCCACCGGC GGCATGGACGAGCTGTACAAGGGAGGTGGGGGATCTGGTGAG GGCAGAGGCAGTCTGCTGACATGCGGTGACGTGGAAGAGAATC CCGGCCCTGGATCCGGCGAGGTGAGTATGGTACATAAAACAAG CATCTATTGAAAATATCTGACAAACTCATCTTTTATTTTTGATGTG TGTGTGTGTGTGTGTGTGTGTGTTTTTTTTTTAACAGGGATTTGGG GAATTATTTGAGAAAGCAAAACAAAACAATAACAATAGAAAAACT TCTAATGGTGATGACAGCACTGCCTGGGTTTCCTGGAAAGAACT CTTATCCCCAGGAACTAGTTTGTTGAATAAATGCTGGTGTGAATG TGAATGGATGATTGAACAGATGAATGAGTGTGATGAGTATGATAA AAGCATGGATGGAGAGATGGGTGAGTACATGGATGGATAGATG GATGAGTTGGTGGGTAGATTCGTGGCTAGATGGATGATGGATGG ATGGATGGATGGATGGATGGATGGACAGATGGATGGATATATGA TTGAACTATTGAAAGTATAGATGTATGGATGGGTGAATTTGGGG GTAATTGTTAGATGATGGATGTGGATGGTTGTGAGTGGCTGGTG GACAGACGAAAAATGGATGGGTGGATAAATTGATGGGTGGATGG ATGGTTGGTTGTATGAAAGAATGAATGATTGGGTAGATAAAAGAG TAGATGAATGAATTAATGAATAAACAGGCAGATGGATGATGTAAG CTGCCCCAGACCCTGGGACCTCTGACCCCCGGCGACCCCTTGC ACTCTCCATGAGCCCTTTCCTTTTTTTTCCTCAGGTCTAGGTGGG GGATCTGGTGAGGGCAGAGGCAGTCTGCTGACATGCGGTGACG TGGAAGAGAATCCCGGCCCTTCTAGAAGCAAGGGCGAGGAGCT GTTCACCGGGGTGGTGCCCATCCTGGTCGAGCTGGACGGCGAC GTAAACGGCCACAAGTTCAGCGTGTCCGGCGAGGGCGAGGGC GATGCCACCTACGGCAAGCTGACCCTGAAGTTCATCTGCACCAC CGGCAAGCTGCCCGTGCCCTGGCCCACCCTCGTGACCACCCTG ACCTACGGCGTGCAGTGCTTCAGCCGCTACCCCGACCACATGA AGCAGCACGACTTCTTCAAGTCCGCCATGCCCGAAGGCTACGTC CAGGAGCGCACCATCTTCTTCAAGGACGACGGCAACTACAAGAC

	CCGCGCCGAGGTGAAGTTCGAGGGCGACACCCTGGTGAACCGC ATCGAGCTGAAGGGCATCGACTTCAAGGAGGACGGCAACATCC TGGGGCACAAGCTGGAGTACAACTACAACAGCCACAACGTCTAT ATCATGGCCGACAAGCAGAAGAACGGCATCAAGGTGAACTTCAA GATCCGCCACAACATCGAGGACGGCAGCGTGCAGCTCGCCGAC CACTACCAGCAGAACACCCCCATCGGCGACGGCCCCGTGCTGC TGCCCGACAACCACTACCTGAGCACCCAGTCCGCCCTGAGCAA AGACCCCAACGAGAAGCGCGATCACATGGTCCTGCTGGAGTTC GTGACCGCCGCCGGGATCACTCTCGGCATGGACGAGCTGTACA AGCTGCAGAGCAGGGCCGACCCCAAGAAGAAGAGGAAGGTGGA CCCCAAGAAGAAGAGGAAGGTGGACCCCAAGAAGAAGAGGAAG GTGTGA
4. Codon-optimized TDP-43	ATGTCTGAATATATTCGGGTAACCGAAGATGAGAACGATGAACC AATCGAAATTCCAAGTGAAGACGACGGAACAGTCTTGCTCTCCA CAGTAACGGCGCAGTTTCCCGGTGCGTGCGGATTGAGATATCG CAACCCGGTGTCTCAGTGCATGCGAGGTGTAAGGTTGGTCGAA GGGATCCTGCACGCCCCCGATGCAGGCTGGGGTAACCTCGTGT ACGTGGTTAACTACCCGAAGGATAACAAGAGGAAAATGGATGAA ACCGATGCTAGTTCCGCCGTGAAGGTGAAACGAGCGGTTCAAAA AACTTCAGATCTTATAGTTCTGGGCCTCCCTTGGAAGACCACGG AACAGGATTTGAAAGAGTATTTTTCAACCTTTGGCGAGGTTCTCA TGGTGCAGGTTAAAAAAGATCTTAAAACCGGACACTCAAAAGGA TTTGGCTTCGTGAGGTTCACCGAGTACGAAACGCAGGTAAAAGT GATGTCACAGCGCCATATGATAGACGGACGGTGGTGCGATTGTA AGCTGCCCAATTCCAAGCAAAGCCAAGACGAGCCTCTGAGGAGT CGCAAAGTTTTCGTTGGACGCTGTACGGAAGACATGACTGAAGA TGAGCTTAGGGAGTTTTTTAGTCAGTATGGAGACGTTATGGATGT CTTTATCCCAAAACCGTTTCGGGCCTTCGCCTTTGTCACCTTTGC CGACGACCAGATCGCCCAGAGCTTGTGTGGCGAAGACCTGATA ATTAAAGGTATATCTGTCCATATCAGCAATGCGGAACCGAAACAC AACTCTAATCGACAGCTTGAGAGGTCAGGGAGGTTTGGGGGTAA CCCGGGTGGATTCGGTAACCAAGGGGGGTTCGGAAACTCCCGG GGCGGAGGAGCCGGATTGGGTAATAACCAGGGATCCAACATGG GCGGCGGGATGAACTTTGGTGCCTTCTCCATAAATCCTGCGATG ATGGCCGCAGCGCAAGCTGCCCTTCAGAGCTCCTGGGGTATGA TGGGGATGCTTGCTTCTCAGCAAAACCAATCCGGGCCCAGCGG CAACAATCAGAATCAAGGTAATATGCAGCGAGAACCGAACCAGG CCTTCGGAAGCGGGAATAATTCCTACTCAGGATCAAATAGTGGT GCAGCCATTGGCTGGGGCTCAGCGTCTAATGCAGGCTCAGGCA

	GTGGGTTTAATGGGGGCTTTGGGAGCTCCATGGACAGCAAGTC ATCAGGCTGGGGGTAA
5. CUTS hSYN1 mScarlet Linker-T2A CFTR_intron 8 CFTR_modifi ed_exon9 UNC13A_mo dified_CE	AGTGCAAGTGGGTTTTAGGACCAGGATGAGGCGGGGTGGGGGT GCCTACCTGACGACCGACCCCGACCCACTGGACAAGCACCCAA CCCCCATTCCCCAAATTGCGCATCCCCTATCAGAGAGGGGGAG GGGAAACAGGATGCGGCGAGGCGCGTGCGCACTGCCAGCTTCA GCACCGCGGACAGTGCCTTCGCCCCCGCCTGGCGGCGCGCGC CACCGCCGCCTCAGCACTGAAGGCGCGCTGACGTCACTCGCCG GTCCCCCGCAAACTCCCCTTCCCGGCCACCTTGGTCGCGTCCG CGCCGCCGCCGGCCCAGCCGGACCGCACCACGCGAGGCGCGA GATAGGGGGGCACGGGCGCGACCATCTGCGCTGCGGCGCCGG CGACTCAGCGCTGCCTCAGTCTGCGGTGGGCAGCGGAGGAGTC GTGTCGTGCCTGAGAGCGCAG

Supplementary Table 1. **Information of DNA sequence**

Acknowledgements

We thank Dr. Yuna Ayala, Ph.D. (St. Louis University School of Medicine), for kindly providing the CFTR minigene plasmids. We thank Dr. Shawn M Ferguson, Ph.D. (Yale University School of Medicine) for kindly providing the TARDBP$^{-/-}$ HeLa cell lines used in this study. We thank Olivia R. Shapiro and Jocelyn C. Mauna (Donnelly Lab, University of Pittsburgh School of Medicine) for their kind assistance and helpful discussions. This work was supported by funds to C.J.D. by the LiveLikeLou Fund at the Pittsburgh Foundation and grants from NIH (R01NS105756, R01NS127187) and R21AG075814 to C.T.C.

Additional information

Authorship contributions

LX, JM, and CAB share equal contributions and authorship. LX and BTH conceptualized the study. LX, JM, and CAB were responsible for data curation, data analysis, conceptualizing and performing the described methodologies, compiling and generating data, and writing the original draft. JX assisted with data analyses and experimental optimization. SB and CTC contributed to experimental design and analysis of the neuronal BE(2)-C studies and edited the manuscript, with SB additionally constructing the stable BE(2)-C lines, conducting the experiments and collecting data. CJD conceptualized the approach, funded the research, and prepared the final manuscript.

Funding

Funder	Grant reference number	Author
HHS | National Institutes of Health (NIH)	R01NS105756	Christopher J Donnelly
HHS | National Institutes of Health (NIH)	R01NS127187	Christopher J Donnelly
HHS | National Institutes of Health (NIH)	R21AG075814	Charleen Chu

Author ORCID iDs

Cristian A Bergmann: https://orcid.org/0000-0001-7564-9742
Christopher J Donnelly: https://orcid.org/0000-0002-2383-9015

References

Aldewachi H, Al-Zidan RN, Conner MT, Salman MM (2021) High-Throughput Screening Platforms in the Discovery of Novel Drugs for Neurodegenerative Diseases. *Bioengineering (Basel)* **8** https://doi.org/10.3390/bioengineering8020030 | PubMed

Ayala YM, Pagani F, Baralle FE (2006) TDP43 depletion rescues aberrant CFTR exon 9 skipping. *FEBS Lett* **580**:1339-1344 https://doi.org/10.1016/j.febslet.2006.01.052 | PubMed

Baughn MW, Melamed Z, López-Erauskin J, Beccari MS, Ling K, Zuberi A, Presa M, Gonzalo-Gil E, Maimon R, Vazquez-Sanchez S, *et al.* (2023) Mechanism of STMN2 cryptic splice-polyadenylation and its correction for TDP-43 proteinopathies. *Science* **379**:1140-1149 https://doi.org/10.1126/science.abq5622 | PubMed

Bock C, Datlinger P, Chardon F, Coelho MA, Dong MB, Lawson KA, Lu T, Maroc L, Norman TM, Song B, *et al.* (2022) High-content CRISPR screening. *Nat Rev Methods Primers* **2** https://doi.org/10.1038/s43586-022-00098-7 | PubMed

Bonet-Ponce L, Beilina A, Williamson CD, Lindberg E, Kluss JH, Saez-Atienzar S, Landeck N, Kumaran R, Mamais A, Bleck CKE, *et al.* (2020) LRRK2 mediates tubulation and vesicle sorting from lysosomes. *Sci Adv* **6** https://doi.org/10.1126/sciadv.abb2454 | PubMed

Brown A-L, Wilkins OG, Keuss MJ, Kargbo-Hill SE, Zanovello M, Lee WC, Bampton A, Lee FCY, Masino L, Qi YA, *et al.* (2022) TDP-43 loss and ALS-risk SNPs drive mis-splicing and depletion of UNC13A. *Nature* **603**:131-137 https://doi.org/10.1038/s41586-022-04436-3 | PubMed

Buratti E, Baralle FE (2001) Characterization and functional implications of the RNA binding properties of nuclear factor TDP-43, a novel splicing regulator of CFTR exon 9. *J Biol Chem* **276**:36337-36343 https://doi.org/10.1074/jbc.M104236200 | PubMed

Cohen TJ, Hwang AW, Restrepo CR, Yuan C-X, Trojanowski JQ, Lee VMY (2015) An acetylation switch controls TDP-43 function and aggregation propensity. *Nat Commun* **6**:5845 https://doi.org/10.1038/ncomms6845 | PubMed

Conicella AE, Dignon GL, Zerze GH, Schmidt HB, D'Ordine AM, Kim YC, Rohatgi R, Ayala YM, Mittal J, Fawzi NL (2020) TDP-43 α-helical structure tunes liquid-liquid phase separation and function. *Proc Natl Acad Sci USA* **117**:5883-5894 https://doi.org/10.1073/pnas.1912055117 | PubMed

Elden AC, Kim H-J, Hart MP, Chen-Plotkin AS, Johnson BS, Fang X, Armakola M, Geser F, Greene R, Lu MM, *et al.* (2010) Ataxin-2 intermediate-length polyglutamine expansions are associated with increased risk for ALS. *Nature* **466**:1069-1075 https://doi.org/10.1038/nature09320 | PubMed

Estades Ayuso V, Pickles S, Todd T, Yue M, Jansen-West K, Song Y, González Bejarano J, Rawlinson B, DeTure M, Graff-Radford NR, *et al.* (2023) TDP-43-regulated cryptic RNAs accumulate in Alzheimer's disease brains. *Mol Neurodegener* **18**:57 https://doi.org/10.1186/s13024-023-00646-z | PubMed

Feldman EL, Goutman SA, Petri S, Mazzini L, Savelieff MG, Shaw PJ, Sobue G (2022) Amyotrophic lateral sclerosis. *Lancet* **400**:1363-1380 https://doi.org/10.1016/S0140-6736(22)01272-7 | PubMed

Huang W-P, Ellis BCS, Hodgson RE, Sanchez Avila A, Kumar V, Rayment J, Moll T, Shelkovnikova TA (2024) Stress-induced TDP-43 nuclear condensation causes splicing loss of function and STMN2 depletion. *Cell Rep* **43**:114421 https://doi.org/10.1016/j.celrep.2024.114421 | PubMed

Hurtle BT, Xie L, Donnelly CJ (2023) Disrupting pathologic phase transitions in neurodegeneration. *J Clin Invest* **133** https://doi.org/10.1172/JCI168549 | PubMed

Jiang L-L, Xue W, Hong J-Y, Zhang J-T, Li M-J, Yu S-N, He J-H, Hu H-Y (2017) The N-terminal dimerization is required for TDP-43 splicing activity. *Sci Rep* **7**:6196 https://doi.org/10.1038/s41598-017-06263-3 | PubMed

Johnson BS, Snead D, Lee JJ, McCaffery JM, Shorter J, Gitler AD (2009) TDP-43 is intrinsically aggregation-prone, and amyotrophic lateral sclerosis-linked mutations accelerate aggregation and increase toxicity. *J Biol Chem* **284**:20329-20339 https://doi.org/10.1074/jbc.M109.010264 | PubMed

Joseph BJ, Marshall KA, Harley P, Mann JR, Alessandrini F, Vanoye CG, Chi W, Prudencio M, Simkin D, Kao T-T, *et al.* (2025) TDP-43-dependent mis-splicing of KCNQ2 triggers intrinsic neuronal hyperexcitability in ALS/FTD. *Nat Neurosci* **28**:2476-2492 https://doi.org/10.1038/s41593-025-02096-w | PubMed

Keating SS, Bademosi AT, San Gil R, Walker AK (2023) Aggregation-prone TDP-43 sequesters and drives pathological transitions of free nuclear TDP-43. *Cell Mol Life Sci* **80**:95 https://doi.org/10.1007/s00018-023-04739-2 | PubMed

Klim JR, Williams LA, Limone F, Guerra San Juan I, Davis-Dusenbery BN, Mordes DA, Burberry A, Steinbaugh MJ, Gamage KK, Kirchner R, *et al.* (2019) ALS-implicated protein TDP-43 sustains levels of STMN2, a mediator of motor neuron growth and repair. *Nat Neurosci* **22**:167-179 https://doi.org/10.1038/s41593-018-0300-4 | PubMed

Koike Y, Pickles S, Estades Ayuso V, Jansen-West K, Qi YA, Li Z, Daughrity LM, Yue M, Zhang Y-J, Cook CN, *et al.* (2023) TDP-43 and other hnRNPs regulate cryptic exon inclusion of a key ALS/FTD risk gene, UNC13A. *PLoS Biol* **21**:e3002028 https://doi.org/10.1371/journal.pbio.3002028 | PubMed

Kuo P-H, Doudeva LG, Wang Y-T, Shen C-KJ, Yuan HS (2009) Structural insights into TDP-43 in nucleic-acid binding and domain interactions. *Nucleic Acids Res* **37**:1799-1808 https://doi.org/10.1093/nar/gkp013 | PubMed

Ling JP, Pletnikova O, Troncoso JC, Wong PC (2015) TDP-43 repression of nonconserved cryptic exons is compromised in ALS-FTD. *Science* **349**:650-655 https://doi.org/10.1126/science.aab0983 | PubMed

Ling S-C, Polymenidou M, Cleveland DW (2013) Converging mechanisms in ALS and FTD: disrupted RNA and protein homeostasis. *Neuron* **79**:416-438 https://doi.org/10.1016/j.neuron.2013.07.033 | PubMed

Lukavsky PJ, Daujotyte D, Tollervey JR, Ule J, Stuani C, Buratti E, Baralle FE, Damberger FF, Allain FH-T (2013) Molecular basis of UG-rich RNA recognition by the human splicing factor TDP-43. *Nat Struct Mol Biol* **20**:1443-1449 https://doi.org/10.1038/nsmb.2698 | PubMed

Lu S, Hu J, Arogundade OA, Goginashvili A, Vazquez-Sanchez S, Diedrich JK, Gu J, Blum J, Oung S, Ye Q, *et al.* (2022) Heat-shock chaperone HSPB1 regulates cytoplasmic TDP-43 phase separation and liquid-to-gel transition. *Nat Cell Biol* **24**:1378-1393 https://doi.org/10.1038/s41556-022-00988-8 | PubMed

Mann JR, Donnelly CJ (2021) RNA modulates physiological and neuropathological protein phase transitions. *Neuron* **109**:2663-2681 https://doi.org/10.1016/j.neuron.2021.06.023 | PubMed

Mann JR, Gleixner AM, Mauna JC, Gomes E, DeChellis-Marks MR, Needham PG, Copley KE, Hurtle B, Portz B, Pyles NJ, *et al.* (2019) RNA Binding Antagonizes Neurotoxic Phase Transitions of TDP-43. *Neuron* **102**:321-338.e8. https://doi.org/10.1016/j.neuron.2019.01.048 | PubMed

Ma XR, Prudencio M, Koike Y, Vatsavayai SC, Kim G, Harbinski F, Briner A, Rodriguez CM, Guo C, Akiyama T, *et al.* (2022) TDP-43 represses cryptic exon inclusion in the FTD-ALS gene UNC13A. *Nature* **603**:124-130 https://doi.org/10.1038/s41586-022-04424-7 | PubMed

McKee AC, Gavett BE, Stern RA, Nowinski CJ, Cantu RC, Kowall NW, Perl DP, Hedley-Whyte ET, Price B, Sullivan C, *et al.* (2010) TDP-43 proteinopathy and motor neuron disease in chronic traumatic encephalopathy. *J Neuropathol Exp Neurol* **69**:918-929 https://doi.org/10.1097/NEN.0b013e3181ee7d85 | PubMed

Mehta PR, Brown A-L, Ward ME, Fratta P (2023) The era of cryptic exons: implications for ALS-FTD. *Mol Neurodegener* **18**:16 https://doi.org/10.1186/s13024-023-00608-5 | PubMed

Melamed Z, López-Erauskin J, Baughn MW, Zhang O, Drenner K, Sun Y, Freyermuth F, McMahon MA, Beccari MS, Artates JW, *et al.* (2019) Premature polyadenylation-mediated loss of stathmin-2 is a hallmark of TDP-43-dependent neurodegeneration. *Nat Neurosci* **22**:180-190 https://doi.org/10.1038/s41593-018-0293-z | PubMed

Nelson PT, Dickson DW, Trojanowski JQ, Jack CR, Boyle PA, Arfanakis K, Rademakers R, Alafuzoff I, Attems J, Brayne C, *et al.* (2019) Limbic-predominant age-related TDP-43 encephalopathy (LATE): consensus working group report. *Brain* **142**:1503-1527 https://doi.org/10.1093/brain/awz099 | PubMed

Neumann M, Sampathu DM, Kwong LK, Truax AC, Micsenyi MC, Chou TT, Bruce J, Schuck T, Grossman M, Clark CM, *et al.* (2006) Ubiquitinated TDP-43 in frontotemporal lobar degeneration and amyotrophic lateral sclerosis. *Science* **314**:130-133 https://doi.org/10.1126/science.1134108 | PubMed

Park S-K, Hong JY, Arslan F, Kanneganti V, Patel B, Tietsort A, Tank EMH, Li X, Barmada SJ, Liebman SW (2017) Overexpression of the essential Sis1 chaperone reduces TDP-43 effects on toxicity and proteolysis. *PLoS Genet* **13**:e1006805 https://doi.org/10.1371/journal.pgen.1006805 | PubMed

Polymenidou M, Lagier-Tourenne C, Hutt KR, Huelga SC, Moran J, Liang TY, Ling S-C, Sun E, Wancewicz E, Mazur C, *et al.* (2011) Long pre-mRNA depletion and RNA missplicing contribute to neuronal vulnerability from loss of TDP-43. *Nat Neurosci* **14**:459-468 https://doi.org/10.1038/nn.2779 | PubMed

Pozzi S, Thammisetty SS, Codron P, Rahimian R, Plourde KV, Soucy G, Bareil C, Phaneuf D, Kriz J, Gravel C, *et al.* (2019) Virus-mediated delivery of antibody targeting TAR DNA-binding protein-43 mitigates associated neuropathology. *J Clin Invest* **129**:1581-1595 https://doi.org/10.1172/JCI123931 | PubMed

Roczniak-Ferguson A, Ferguson SM (2019) Pleiotropic requirements for human TDP-43 in the regulation of cell and organelle homeostasis. *Life Sci Alliance* **2** https://doi.org/10.26508/lsa.201900358 | PubMed

Schmidt HB, Barreau A, Rohatgi R (2019) Phase separation-deficient TDP43 remains functional in splicing. *Nat Commun* **10**:4890 https://doi.org/10.1038/s41467-019-12740-2 | PubMed

Shin JE, Geisler S, DiAntonio A (2014) Dynamic regulation of SCG10 in regenerating axons after injury. *Exp Neurol* **252**:1-11 https://doi.org/10.1016/j.expneurol.2013.11.007 | PubMed

Shin JE, Miller BR, Babetto E, Cho Y, Sasaki Y, Qayum S, Russler EV, Cavalli V, Milbrandt J, DiAntonio A (2012) SCG10 is a JNK target in the axonal degeneration pathway. *Proc Natl Acad Sci USA* **109**:E3696-705 https://doi.org/10.1073/pnas.1216204109 | PubMed

Sun M, Bell W, LaClair KD, Ling JP, Han H, Kageyama Y, Pletnikova O, Troncoso JC, Wong PC, Chen LL (2017) Cryptic exon incorporation occurs in Alzheimer's brain lacking TDP-43 inclusion but exhibiting nuclear clearance of TDP-43. *Acta Neuropathol* **133**:923-931 https://doi.org/10.1007/s00401-017-1701-2 | PubMed

Tremblay C, St-Amour I, Schneider J, Bennett DA, Calon F (2011) Accumulation of transactive response DNA binding protein 43 in mild cognitive impairment and Alzheimer disease. *J Neuropathol Exp Neurol* **70**:788-798 https://doi.org/10.1097/NEN.0b013e31822c62cf | PubMed

Tseng Y-L, Lu P-C, Lee C-C, He R-Y, Huang Y-A, Tseng Y-C, Cheng T-JR, Huang JJ-T, Fang J-M (2023) Degradation of neurodegenerative disease-associated TDP-43 aggregates and oligomers via a proteolysis-targeting chimera. *J Biomed Sci* **30**:27 https://doi.org/10.1186/s12929-023-00921-7 | PubMed

Varoqueaux F, Sigler A, Rhee J-S, Brose N, Enk C, Reim K, Rosenmund C (2002) Total arrest of spontaneous and evoked synaptic transmission but normal synaptogenesis in the absence of Munc13-mediated vesicle priming. *Proc Natl Acad Sci USA* **99**:9037-9042 https://doi.org/10.1073/pnas.122623799 | PubMed

Wilkins OG, Chien MZYJ, Wlaschin JJ, Barattucci S, Harley P, Mattedi F, Mehta PR, Pisliakova M, Ryadnov E, Keuss MJ, *et al.* (2024) Creation of de novo cryptic splicing for ALS and FTD precision medicine. *Science* **386**:61-69 https://doi.org/10.1126/science.adk2539 | PubMed

Willemse SW, Harley P, van Eijk RPA, Demaegd KC, Zelina P, Pasterkamp RJ, van Damme P, Ingre C, van Rheenen W, Veldink JH, *et al.* (2023) UNC13A in amyotrophic lateral sclerosis: from genetic association to therapeutic target. *J Neurol Neurosurg Psychiatr* **94**:649-656 https://doi.org/10.1136/jnnp-2022-330504 | PubMed

Xia X, Zhang Y, Zieth CR, Zhang S-C (2007) Transgenes delivered by lentiviral vector are suppressed in human embryonic stem cells in a promoter-dependent manner. *Stem Cells Dev* **16**:167-176 https://doi.org/10.1089/scd.2006.0057 | PubMed

Yang C, Qiao T, Yu J, Wang H, Guo Y, Salameh J, Metterville J, Parsi S, Yusuf I, Brown RH, *et al.* (2022) Low-level overexpression of wild type TDP-43 causes late-onset, progressive neurodegeneration and paralysis in mice. *PLoS ONE* **17**:e0255710 https://doi.org/10.1371/journal.pone.0255710 | PubMed

Yu H, Lu S, Gasior K, Singh D, Vazquez-Sanchez S, Tapia O, Toprani D, Beccari MS, Yates JR, Da Cruz S, *et al.* (2021) HSP70 chaperones RNA-free TDP-43 into anisotropic intranuclear liquid spherical shells. *Science* **371** https://doi.org/10.1126/science.abb4309 | PubMed

Zhang X, Das T, Chao TF, Trinh V, Carmen-Orozco RP, Ling JP, Kalab P, Hayes LR (2024) Multivalent GU-rich oligonucleotides sequester TDP-43 in the nucleus by inducing high molecular weight RNP complexes. *iScience* **27**:110109 https://doi.org/10.1016/j.isci.2024.110109 | PubMed

Peer reviews

Reviewer #2 (Public review):

Summary:

The authors goals is to be develop a more accurate system that reports TDP-43 activity as a splicing regulator. Prior to this, most methods employed western blotting or QPCR based assays to determine whether targets of TDP-43 were up or down regulated. The problem with

that is the sensitivity. This approach uses an ectopic delivered construct containing splicing elements from CFTR and UNC13A (two known splicing targets) fused to a GFP reporter. Not only does it report TDP-43 function well, but it operates at extremely sensitive TDP-43 levels, requiring only picomolar TDP-43 knockdown for detection. This reporter should supersede the use of current TDP-43 activity assays, its cost-effective, its rapid and reliable.

Strengths:

In general, the experiments are convincing and well designed. The rigor, number of samples and statistics, and gradient of TDP-43 knockdown were all viewed as strengths. In addition, the use of multiple assays to confirm the splicing changes were viewed as complimentary (ie PCR and GFP-fluorescence) adding additional rigor. The final major strength i'll add is the very clever approach to tether TDP-43 to the loss of function cassette such that when TDP-43 is inactive it would autoregulate and induce wild-type TDP-43. This has many implications for the use of other genes, not just TDP-43, but also other protective factors that may need to be re-established upon TDP-43 loss of function.

Weaknesses:

Admittedly, one needs to initially characterize the sensor and the use of cell lines is an obvious advantage, but it begs the question of whether this will work in neurons. Additional future experiments in primary neurons will be needed. The bulk analysis of GFP-positive cells is a bit crude. As mentioned in the manuscript, flow sorting would be an easy and obvious approach to get more accurate homogenous data. This is especially relevant since the GFP signal is quite heterogenous in the image panels, for example Figure 1C, meaning the siRNA is not fully penetrant. Therefore, stating that 1% TDP-43 knockdown achieves the desired sensor regulation might be misleading. Flow sorting would provide a much more accurate quantification of how subtle changes in TDP-43 protein levels track with GFP fluorescence.

Some panels in the manuscript would benefit from additional clarity to make the data easier to visualize. For example, Figure 2D and 2G could be presented in a more clear manner, possibly split into additional graphs since there are too many outputs. Sup Figure 2A image panels would benefit from being labeled, its difficult to tell what antibodies or fluorophores were used. Same with Figure 4B.

Figure 3 is an important addition to this manuscript and in general is convincing showing that TDP-43 loss of function mutants can alter the sensor. However, there is still wild-type endogenous TDP-43 in these cells, and its unclear whether the 5FL mutant is acting as a dominant negative to deplete the total TDP-43 pool, which is what the data would suggest. This could have been clarified. Additional treatment with stressors that inactivate TDP-43 could be tested in future studies.

Overall, the authors definitely achieved their goals by developing a very sensitive readout for TDP-43 function. The results are convincing, rigorous, and support their main conclusions. There are some minor weaknesses listed above, chief of which is the use of flow sorting to improve the data analysis. But regardless, this study will have an immediate impact for those who need a rapid, reliable, and sensitive assessment of TDP-43 activity, and it will be particularly impactful once this reporter can be used in isolated primary cells (ie neurons) and in vivo in animal models. Since TDP-43 loss of function is thought to be a dominant pathological mechanism in ALS/FTD and likely many others disorders, having these type of sensors is a major boost to field and will change our ability to see sub-threshold changes in TDP-43 function that might otherwise not be possible with current approaches.

Comments on revisions:

In the revised version, most of the reviewer's comments have been appropriately addressed with the exception of 1) the use of flow sorting to improve the data analysis and 2) testing this sensor in primary neurons. The latter is the focus of an ongoing separate study. Though flow sorting would significantly strengthen this study and help others in the field to use this sensor, it is still an impactful and innovative study without it.

https://doi.org/10.7554/eLife.101216.2.sa2

Reviewer #3 (Public review):

The DNA and RNA binding protein TDP-43 has been pathologically implicated in a number of neurodegenerative diseases including ALS, FTD, and AD. Normally residing in the nucleus, in TDP-43 proteinopathies, TDP-43 mislocalizes to the cytoplasm where it is found in cytoplasmic aggregates. It is thought that both loss of nuclear function and cytoplasmic gain of toxic function are contributors to disease pathogenesis in TDP-43 proteinopathies. Recent studies have demonstrated that depletion of nuclear TDP-43 leads to loss of its nuclear function characterized by changes in gene expression and splicing of target mRNAs. However, to date, most readouts of TDP-43 loss of function events are dependent upon PCR based assays for single mRNA targets. Thus, reliable and robust assays for detection of global changes in TDP-43 splicing events are lacking. In this manuscript, Xie, Merjane, Bergmann and colleagues describe a biosensor that reports on TDP-43 splicing function in real time. Overall, this is a well-described unique resource that would be of high interest and utility to a number of researchers validated in multiple cell types as a sensitive readout of TDP-43 loss of function. Future studies validating the utility of this biosensor in models of TDP-43 loss of function (e.g. disease iPSNs) that do not rely on TDP-43 knockdown will be of further interest.

https://doi.org/10.7554/eLife.101216.2.sa1

Author Response:

The following is the authors' response to the previous reviews

> ***Public Review:***

We thank the editor and reviewers for their thoughtful and constructive feedback, which has enabled us to greatly strengthen the manuscript. We apologize for the delay in resubmitting this as we were dealing with a large turnover in the lab due to trainee graduations which has We have carefully revised the text, figures, and supplementary materials in response to these comments. Below, we summarize the key revisions made followed by a point-by-point response to the reviewers' critiques.

(1) Performed CUTS analyses in human neuronal system: In the revised manuscript, we included new data demonstrating that the CUTS system can be applied to additional cellular models, specifically neuronal cells (Figure 5, Figure S4). To address whether CUTS functions effectively in neuronal contexts, we generated stable CUTS-expressing lines in differentiated BE(2)-C and ReN VM–derived differentiated neurons (Figure 5A-D, Figure S4 A-C). To ensure this was neuronal expression, we developed a new Tet-On3G system construct where the Tet-On3G transactivating protein is driven by the SYN1 promoter to ensure neuron-specific inducible expression for these experiments.

(2) Define the relationship between CUTS and endogenous/physiological cryptic exons inclusion: To evaluate how well the CUTS system reflects physiological cryptic exon regulation, we performed RT-PCR analysis of several cryptic exons previously reported by us and evaluated CUTS activation at the RNA level in parallel (Figure S2E) . CUTS is sensitive to

low-mild reductions in TDP-43 levels, whereas the tested endogenous cryptic exons exhibit variable responses to TDP-43 knockdown.

(3) Defining stress-induced TDP-43 loss of function: We included new data demonstrating that the CUTS system can detect TDP-43 loss of function induced by acute sodium arsenite ($NaAsO_2$) treatment in HEK cells (Figure 3D–I). We have also tested additional stressor as part of a separate ongoing study where this work will be expanded upon (Xie et al., 2025). We selected this paradigm since TDP-43 loss of function in response to acute $NaAsO_2$ treatment is also supported by work from other labs(Huang et al., 2024).

(4) Implications of using a TDP-43 Loss-of-Function sensor for therapeutic applications: In the revised manuscript, we clarify that CUTS-TDP43 is auto-regulated and we highlight two potential therapeutic applications: i) TDP-43 Knockdown-and-replacement: CUTS-TDP43 provides a strategy for simultaneous depletion of pathological TDP-43 species while enabling autoregulated re-expression of wild-type TDP-43. This design mitigates the risk of supraphysiologic overexpression, a known liability in conventional replacement approaches, by restoring TDP-43 within a self-limiting regulatory network that maintains homeostatic control. ii) Aggregation-independent correction: Because CUTS is autoregulatory, it can be repurposed to regulate alternative downstream effectors, including splicing modifiers or TDP-43 functional interactors, without expressing TDP-43 itself. This approach provides a potential aggregation-independent strategy to compensate for TDP-43 loss-of-function (LOF) by restoring downstream splicing. We are evaluating this work in a follow up study (Xie et al., 2025). In these ongoing studies, we show that CUTS-regulated expression of splicing proteins in response to TDP-43 loss restored subsets of cryptic exon events (24/28 events evaluated). These findings suggest CUTS as a versatile tool for both autoregulated TDP-43 replacement and trans-regulatory therapeutic correction. We expanded on this concept in the discussion section of this revised manuscript. We also note that autoregulatory TDP-43 biosensor strategies have been proposed in related systems, including TDP-Reg, underscoring broader interest in self-regulated TDP-43 systems (Wilkins et al., 2024).

(5) Clarified mechanism of TDP-43 5FL causing strong loss of function: The TDP-43 5FL exhibits reduced RNA binding capacity, and we previously showed that the lack of RNA binding promotes aberrant homotypic phase separation of TDP-43 (Mann et al., 2019). Expression of RNA-deficient TDP-43 variant forms nuclear “anisomes” (Yu et al., 2021), which evidence suggests sequesters endogenous TDP-43 protein into insoluble structures. We expanded on this in our results section in this revised manuscript.

(6) Improved figure clarity and data presentation: To enhance clarity and organization, we maintained the main structure of the manuscript while reorganizing figures and improved data visualization. Some examples include:

Figure 1: We revised the schematic layout for greater clarity and simplicity. The figure now focuses more specifically on the CUTS data, with additional data on the UNC13A-TS and CFTR-TS moved to Figure S1. To improve readability, titles were added to all schematic panels. Visual consistency was also improved by refining the color labelling for each sensor in Figures 1C and 1D and adjusting the corresponding bar graphs accordingly.

Figure 2: We reorganized the figure to clearly distinguish between protein and mRNA analyses for greater clarity. In the revised layout, western blot quantifications of TDP-43 and CUTS (GFP) signals are shown in Figures 2D and 2E, respectively, while the corresponding qPCR analyses are presented in Figures 2H and 2I. Minor edits include removing the percentage knockdown and fold-change annotations from the graphs and incorporating these values into a mini-table in Figure S2E.

The original Figure 2D and 2G were reincorportated as reference panels in Figure S2A–B, while new graphs showing CUTS protein-level changes as a function of TDP-43 knockdown

were added (Figure S2C–D). We also incorporated new data showing the behavior of endogenous cryptic exons under low siTDP-43 treatment (Figure S2E).

Figure 3: We added new data demonstrating that the application of the CUTS system in detecting TDP-43 loss of function induced by stress conditions. Specifically, we show that sodium arsenite ($NaAsO_2$) treatment leads to TDP-43 functional impairment detectable by CUTS and supported with endogenous cryptic exon via RT-PCR (Figure 3D-I).

Figure 5 and Figure S4: We introduced a new figure that demonstrates the effective application of the CUTS system in differentiated neuronal systems, thereby extending its usability to disease-relevant cell types.

Figures 2SA and 4B were edited to include the corresponding labels on the sides of each image for clarity. Sup Figure 2A was moved to Sup Figure 3A, while Figure 4B remains in its original configuration.

We thank the reviewers again for their insightful critiques and helpful suggestions, which have enabled us to substantially improve the manuscript. Please find our detailed response to each review below:

> ***Reviewer #1 (Public review):***
>
> *Summary:*
>
> *The authors create an elegant sensor for TDP -43 loss of function based on cryptic splicing of CFTR and UNC13A. The usefulness of this sensor primarily lies in its use in eventual high throughput screening and eventual in vivo models. The TDP-43 loss of function sensor was also used to express TDP-43 upon reduction of its levels.*
>
> *Strengths:*
>
> *The validation is convincing, the sensor was tested in models of TDP-43 loss of function, knockdown and models of TDP-43 mislocalization and aggregation. The sensor is susceptible to a minimal decrease of TDP-43 and can be used at the protein level unlike most of the tests currently employed,*
>
> *Weaknesses:*
>
> *Although the LOF sensor described in this study may be a primary readout for high-throughput screens, ALS/TDP-43 models typically employ primary readouts such as protein aggregation or mislocalization. The information in the two following points would assist users in making informed choices.*
>
> *(1) Testing the sensor in other cell lines*

We thank the reviewer for raising this important point. In agreement with this suggestion, we generated ReN VM cell lines and used a neuroblastoma cell line model (BE(2)-C) expressing the TetOn3G CUTS system under a human synapsin I (hSYN1) promoter. In this construct the transactivator protein is under the control of a neuronal specific hSYN1 promoter whereas the classical TetOn3G system uses a CMV-like promoter. Several studies have reported reduced activity or silencing of CMV and PGK-driven transgenes in neurons. Therefore, we for our neuronal experiments, we removed this promoter to generate a new version of a doxycycline-inducible CUTS system in which Tet-On 3G transactivator is now driven by the hSYN1 promoter which will express CUTS in response to doxycycline treatment. In this improved construct, we also replaced mCherry with mScarlet to enhance the fluorescent signal.

To test this neuronal-adapted system, we established stable CUTS expression in undifferentiated BE(2)-C cells, a subclone of the SK-N-BE(2) neuroblastoma line that has been used to study TDP-43–dependent splicing function(Brown et al., 2022). This model can be differentiated into neuron-like cells within 10 days, as shown in Supplementary Figure 4A. Using this model, we confirmed that TDP-43 knockdown leads to robust activation of the CUTS system (Figure 5B-E). We additionally tested this in in a stable polyclonal ReN VM cells following differentiation into cortical-like neurons (Figure 5D, Figure S4B-C).

> *(2) Establishing a correlation between the sensor's readout and the loss of function (LOF) in the physiological genes would be useful given that the LOF sensor is a hybrid structure and doesn't represent any physiological gene. It would be beneficial to determine if a minor decrease (e.g., 2%) in TDP-43 levels is physiologically significant for a subset of exons whose splicing is controlled by TDP43.*

We agree with the reviewer that correlating the sensor's readout with physiological TDP-43 splicing targets is essential to validate its biological relevance. To this end, we complemented our sensor expression profile with endogenous cryptic exons (CEs) sensitive to TDP-43 depletion. We tested a panel of five physiological cryptic exons regulated by TDP-43 (LRP8, EPB41L4A, ARHGAP32, HDGFL2, and ACBD3). To address the reviewer's concerned, we performed RT-PCR on samples from the low-dose siTDP-43 experiment shown in Figure S2E.

The endogenous CEs used in the panel were selected based on our own and others' preliminary observations. Among these, HDGFL2 showed a particularly robust increase in cryptic exon inclusion at very low siTDP-43 concentrations (38 pM), while untreated samples showed almost no CE inclusion. This finding strongly supports a direct mechanism linking mild TDP-43 reduction to loss of physiological splicing control.

> *(3) Considering that most TDP-LOF pathologically occurs due to aggregation and or mislocalization, and in most cases the endogenous TDP-43 gene is functional but the protein becomes non-functional, the use of the loss of function sensor as a switch to produce TDP-43 and its eventual use as gene therapy would have to contend with the fact that the protein produced may also become nonfunctional. This would eventually be easy to test in one of the aggregation modes that were used to test the sensor.. However, as the authors suggest, this is a very interesting system to deliver other genetic modifiers of TDP-43 proteinopathy in a regulated fashion and timely fashion.*

We thank the reviewer for this thoughtful point and agree that in the disease-relevant context where endogenous TDP-43 is intact but TDP-43 function is lost due to mislocalization and/or aggregation, a re-supply of TDP-43 risks sequestration and loss of activity. In our manuscript, the CUTS-TDP43 module was presented as a control circuit proof-of-concept rather than a stand-alone approach: it demonstrates that CUTS can (i) sense LOF with high dynamic range and proportionality, and (ii) drive a payload under negative feedback such that total TDP-43 remains near baseline while partially rescuing a splicing readout (CFTR minigene) under knockdown conditions.

Importantly, we evaluated CUTS in aggregation/mislocalization-prone contexts: ΔNLS, 5FL, and ΔNLS+5FL variants trigger CUTS activation (ref), allowing us to quantify LOF arising from these aggregation modes. This confirms that CUTS can operate precisely in the very settings where sequestration is likely to occur.

To directly address the reviewer's suggestion, in the revision we (i) clarify in the Discussion that CUTS-TDP43 is a circuit demonstration and not our proposed monotherapy in aggregation-dominant disease; and (ii) expand our therapeutic framing into two approaches:

Knockdown-and-replacement: concurrently deplete aggregation-prone/endogenous pathologic TDP-43 species (i.e., mutant TDP-43) while using CUTS to re-deliver wild-type TDP-

43 under autoregulation. Aggregation-independent correction: use of CUTS to deliver modifiers that bypass TDP-43 sequestration (e.g., downstream effectors or splicing correctors that restore LOF consequences without expressing TDP-43 itself).

> *(4) I don't think the quantity of siRNA is directly proportional to the degree of TDP-43 knockdown/extent of TDP-43 loss. Therefore, to enhance the utility of the dose-response curves, I'd suggest using TDP-43 levels as the variable on the x-axis, rather than the amount of siRNA administered or even just adding a plot alongside the current plots would enable readers to quickly evaluate LOF response levels concerning the protein. While I understand that the sensitivity of Western blots for quantification might be why the authors have not created the graphs in this manner, having this information would be useful.*

We appreciate the reviewer's insightful comment. As noted, in the original version of the graph, we incorporated the percentage of TDP-43 knockdown corresponding to each siTDP-43 concentration (indicated in red text). However, we agree that this format was not easy to interpret, given the amount of information presented. To address this, we generated two new plots in which the x-axis represents TDP-43 levels (percentage of remaining protein or mRNA), and the y-axis shows the fold change in CUTS signal measured by (i) TDP-43 protein pixel intensity and (ii) TDP-43 mRNA levels, respectively. These new plots are now included as Supplementary Figures 2C–D, which allow a clearer visualization of CUTS readout in relation to actual TDP-43 levels rather than siRNA dose. As the reviewer anticipated, the reason we did not originally present the data in this format was that at low siTDP-43 concentrations, the fold change is minimal and more difficult to quantify by Western blot. Nevertheless, we have now incorporated the revised plots to strengthen the interpretation of the dose–response relationship. Additionally, we experience batch effects across siRNA lots. We believe this revised format should enhance the clarity of the result.

> *(5) p3 line 74: one of the reasons cited as a pitfall of using the endogenous cryptic exons exhibit variable responses to TDP-43 loss and may be cell type-specific. has the sensor been used in different cell lines?*

We tested the CUTS system in differentiated neuronal models using two differentiated neuronal cell types, BE(2)C and ReN VM cells. The results are presented in Figure 5 and Figure S4 of the revised manuscript.

> *(6) The order of the text describing 1A and 1B is confusing. The text starts describing the TS cassettes referring to 1A using the CUTS cassettes which haven't been introduced yet as an example. I'd suggest reorganising this section. The graph, always in 1A showing readout proportional to GFP should be taken out or highlighted in the figure legend that it is theoretical.*

We agree with the reviewer's point. In the original schematic (Figure 1A), we included the CUTS system as an example to introduce the TS cassette design, since it contains the three possible sensor configurations. However, we recognize that this could be confusing. Therefore, we have removed the CUTS cassette from Figure 1A, along with the theoretical graph showing GFP readout proportional to the degree of TDP-43 LOF. In agreement with this change, we also restructured Figure 1. As the focus is the CUTS system, we have moved the Western blot and quantification of UNC13A-TS and CFTR-TS to Supplementary Figure 1.

> ***Reviewer #2 (Public review):***
>
> *Summary:*
>
> *The authors goal is to develop a more accurate system that reports TDP-43 activity as a splicing regulator. Prior to this, most methods employed western blotting or QPCR-based assays to determine whether targets of TDP-43 were up or down-regulated. The problem*

> *with that is the sensitivity. This approach uses an ectopic delivered construct containing splicing elements from CFTR and UNC13A (two known splicing targets) fused to a GFP reporter. Not only does it report TDP-43 function well, but it operates at extremely sensitive TDP-43 levels, requiring only picomolar TDP-43 knockdown for detection. This reporter should supersede the use of current TDP-43 activity assays, it's cost-effective, rapid and reliable.*
>
> *Strengths:*
>
> *In general, the experiments are convincing and well designed. The rigor, number of samples and statistics, and gradient of TDP-43 knockdown were all viewed as strengths. In addition, the use of multiple assays to confirm the splicing changes were viewed as complimentary (ie PCR and GFPfluorescence) adding additional rigor. The final major strength I'll add is the very clever approach to tether TDP-43 to the loss of function cassette such that when TDP-43 is inactive it would autoregulate and induce wild-type TDP-43. This has many implications for the use of other genes, not just TDP-43, but also other protective factors that may need to be re-established upon TDP-43 loss of function.*
>
> *Weaknesses:*
>
> *(1) Admittedly, one needs to initially characterize the sensor and the use of cell lines is an obvious advantage, but it begs the question of whether this will work in neurons. Additional future experiments in primary neurons will be needed.*

We thank the reviewer for highlighting the importance of validating the sensor in neuronal models, given the central role of TDP-43 dysfunction in ALS/FTD and related neurodegenerative disorders. While initial characterization in established cell lines provides experimental control and scalability, we agree that demonstrating functionality in neuronal systems is essential. To address this, we adapted the CUTS platform for neuronal application by incorporating the human synapsin-1 (hSYN1) promoter into the Tet-On 3G system to enable inducible, neuronal specific expression. We validated this configuration in differentiated BE(2)-C cells (Figures 5A-C, S4A-C), where CUTS retained robust responsiveness to TDP-43 perturbation. In parallel, we generated stable CUTS-expressing ReN VM neural progenitor cells and differentiated them for three weeks prior to functional assessment (Figures 5A-C, S4A-C). In both neuronal models, CUTS was functional and responsive to TDP-43 siRNA. We are currently optimizing promoter selection and expression paradigms for fully differentiated iPSC-derived neuronal models and will be the subject of future studies.

> *(2) The bulk analysis of GFP-positive cells is a bit crude. As mentioned in the manuscript, flow sorting would be an easy and obvious approach to get more accurate homogenous data. This is especially relevant since the GFP signal is quite heterogeneous in the image panels, for example, Figure 1C, meaning the siRNA is not fully penetrant. Therefore, stating that 1% TDP-43 knockdown achieves the desired sensor regulation might be misleading. Flow sorting would provide a much more accurate quantification of how subtle changes in TDP-43 protein levels track with GFP fluorescence.*

We thank the reviewer for this thoughtful suggestion. We agree that flow cytometry and sorting of GFP-positive populations would provide a higher-resolution, single-cell–level relationship between TDP-43 abundance and sensor output. Such an approach would reduce heterogeneity arising from incomplete siRNA penetrance and allow more precise quantification of how incremental changes in TDP-43 protein levels track with GFP fluorescence. In the present study, our goal was to establish proof-of-principle functionality of the CUTS circuit and to demonstrate that graded TDP-43 depletion produces a proportional sensor response at the population level. While GFP signal heterogeneity is visible in imaging panels, we hypothesize that this variability likely reflects known differences in siRNA uptake and transfection efficiency rather than instability of the circuit itself. Importantly, bulk

measurements consistently demonstrated dose-dependent sensor regulation across independent experiments, supporting the robustness of the system despite cellular heterogeneity. Furthermore, we were able to quantify CUTS activation in HeLa TARDBP$^{-/-}$ cells. We also note that CUTS was developed as a practical tool for rapid assessment of TDP-43 LOF in standard laboratory settings. Although flow cytometry increases resolution, the ability to detect functional perturbation using bulk fluorescence measurements supports the utility of the system for routine and high-throughput applications.

We agree that flow cytometry would provide a more refined analysis of the dynamic range and sensitivity of CUTS, particularly for defining thresholds such as minimal TDP-43 knockdown required for measurable activation. We plan to include this work in future studies. Specifically, we have implemented FACs sorting of CUTS-expressing cells in a parallel study in which we are conducting a CRISPR knockout screen to identify modifiers of TDP-43 splicing function. For this, we incorporate TDP-43 knockdown followed by FACs to stratify cells based on CUTS activation. This strategy enables direct evaluation of the relationship between the extent of TDP-43 LOF and CUTS sensor activation. These analyses are ongoing and provide a more quantitative analyses linking TDP-43 depletion to CUTS activation and address the reviewer's concern regarding heterogeneity in bulk measurements. We plan to include this in a future study.

> *(3) Some panels in the manuscript would benefit from additional clarity to make the data easier to visualize. For example, Figure 2D and 2G could be presented in a more clear manner, possibly split into additional graphs since there are too many outputs.*

We thank the reviewer for this suggestion. In response, we have split the graphs previously shown in Figures 2D and 2G to improve clarity, as we agree that these panels contained an extensive amount of data. We Specifically split Figure 2D into two separate graphs showing TDP-43 and GFP pixel intensity from Western blots on the Y-axis, plotted against low siTDP-43 treatment on the X-axis. Please see this data as Figure 2 D and Figure 2E in the new manuscript.

Furthermore, for Figure 2G we also split into graphs showing the fold change of mRNA for TDP-43 and the CUTS cryptic exon plotted against low siTDP-43 treatment on the X-axis. Please see this data as Figure 2 H and Figure 2I in the new manuscript. We have maintained the previous graphs in Supplementary Figure 2 to preserve the full dataset for reference.

> *(4) Sup Figure 2A image panels would benefit from being labeled, its difficult to tell what antibodies or fluorophores were used. Same with Figure 4B.*

We appreciate the reviewer's careful observation. In both figures, we are showing mCherry and GFP signals. In the revised version, we have added the corresponding labels to the side of each image for clarity. Therefore, Sup Figure 2A has been moved and is now Sup Figure 3A, while Figure 4B remains in its original configuration.

> *(5) Figure 3 is an important addition to this manuscript and in general is convincing showing that TDP43 loss of function mutants can alter the sensor. However, there is still wild-type endogenous TDP-43 in these cells, and it's unclear whether the 5FL mutant is acting as a dominant negative to deplete the total TDP-43 pool, which is what the data would suggest. This could have been clarified.*

The TDP-43 5FL variant exhibits reduced RNA-binding capacity, and we previously demonstrated that impaired RNA binding promotes aberrant homotypic phase separation of TDP-43. Consistent with this mechanism, expression of RNA-binding–deficient TDP-43 variants induces the formation of nuclear "anisomes" which have been shown to sequester endogenous TDP-43 into insoluble fractions via dominant-negative mechanisms (Cohen et al., 2015; Keating et al., 2023; Mann et al., 2019; Yu et al., 2021). These findings support a model in

which disruption of RNA engagement alters TDP-43 biophysical behavior and promotes functional depletion through self-association. We have expanded this mechanistic explanation in the Results section of the revised manuscript to better contextualize the behavior of the 5FL construct and its impact on endogenous TDP-43.

> *(6) Additional treatment with stressors that inactivate TDP-43 could be tested in future studies.*

We appreciate this suggestion and agree with this important point. Due to the lack of methods to directly induce endogenous TDP-43 aggregation and loss of function, the use of stressors has become a partial solution to address this issue. In line with this, our group has tested several stressors in follow-up research, including sodium arsenite ($NaAsO_2$), puromycin, KCl, MG132, sorbitol, and tunicamycin, using HEK cells expressing the CUTS system(Xie et al., 2025). We were able to show a dose-response relationship in relative GFP intensity under these conditions, with sodium arsenite showing the strongest effect, consistent with previous reports(Huang et al., 2024). To provide additional relevant findings in the current manuscript, we expanded this analysis by testing sodium arsenite in the CUTS system while also including endogenous cryptic exons. We therefore added a new figure showing the effect of sodium arsenite on the CUTS system, including GFP intensity measurements, qPCR using CUTS cryptic exon primers, and three endogenous cryptic exon reporters (ATG4B, GPSM2, and KCNQ2).

> *Overall, the authors definitely achieved their goals by developing a very sensitive readout for TDP-43 function. The results are convincing, rigorous, and support their main conclusions. There are some minor weaknesses listed above, chief of which is the use of flow sorting to improve the data analysis. But regardless, this study will have an immediate impact for those who need a rapid, reliable, and sensitive assessment of TDP-43 activity, and it will be particularly impactful once this reporter can be used in isolated primary cells (ie neurons) and in vivo in animal models. Since TDP-43 loss of function is thought to be a dominant pathological mechanism in ALS/FTD and likely many other disorders, having these types of sensors is a major boost to the field and will change our ability to see sub-threshold changes in TDP-43 function that might otherwise not be possible with current approaches.*
>
> *(7) Regarding the methods, they seem a bit sparse and would benefit from additional detail. For example, I do not see a section in the methods where microscopy images were quantified (%GFP positive cells for example). This information is important and is lacking in the current form.*

We thank the reviewers, and we add the following information in the method section: For live imaging quantification, we measured the mean GFP signal intensity for each group. The values were averaged, and the fold change was calculated and plotted. For immunofluorescent imaging, we first created maximum intensity projection images. We then applied masks to the GFP, mCherry, and Hoechst signals. By overlapping the GFP and mCherry signals, we identified the number of GFP-positive cells. Similarly, by overlapping the mCherry signal with the Hoechst mask, we identified the CUTS-expressing cells. We then calculated the ratio of GFPpositive cells to CUTS-expressing cells and plotted it as a percentage of GFP-positive cells. All analyses were performed using the Nikon NIS software. This information is included in the methods of the revised manuscript.

> ***Reviewer #3 (Public review):***
>
> *The DNA and RNA binding protein TDP-43 has been pathologically implicated in a number of neurodegenerative diseases including ALS, FTD, and AD. Normally residing in the nucleus, in TDP-43 proteinopathies, TDP-43 mislocalizes to the cytoplasm where it is found in cytoplasmic aggregates. It is thought that both loss of nuclear function and cytoplasmic gain of toxic function are contributors to disease pathogenesis in TDP-43*

> *proteinopathies. Recent studies have demonstrated that depletion of nuclear TDP-43 leads to loss of its nuclear function characterized by changes in gene expression and splicing of target mRNAs. However, to date, most readouts of TDP-43 loss of function events are dependent upon PCR-based assays for single mRNA targets. Thus, reliable and robust assays for detection of global changes in TDP-43 splicing events are lacking. In this manuscript, Xie, Merjane, Bergmann and colleagues describe a biosensor that reports on TDP-43 splicing function in real time. Overall, this is a well described unique resource that would be of high interest and utility to a number of researchers. Nonetheless, a couple of points should be addressed by the authors to enhance the overall utility and applicability of this biosensor.*
>
> *(1) While the rationale for selecting UNC13A CE as the reporting CE species is understood given the relevance to disease, could the authors please comment on whether other CE sequences would behave similarly or as robustly? This is particularly critical given the multitude of different splicing changes that can occur as a result of TDP-43 loss of function (ie cryptic exons of differing sensitivity, skiptic exons, premature polyadenylation).*

We thank the reviewer for this question regarding generalizability beyond the UNC13A CE. While UNC13A was selected due to its strong disease relevance and well-characterized sensitivity to TDP-43 loss-of-function (LOF), our platform is not intrinsically restricted to this sequence. In the manuscript, we directly compared three architectures: UNC13A-TS, CFTR-TS, and the combined CUTS sensor incorporating additional UG motif optimization. Under matched conditions in stable HEK293 lines, CUTS demonstrated superior specificity and sensitivity, exhibiting near-zero baseline activity and a proportional, log-linear response across low-dose siTDP43 (38–1200 pM) (Figures 1–2). Importantly, this head-to-head comparison demonstrates that sensor performance can be engineered and optimized beyond a single CE species.

TDP-43 LOF is known to induce a spectrum of RNA processing defects, including cryptic exons with differing sensitivities and cell-type dependence, premature polyadenylation events (e.g., STMN2), and, under conditions of excess nuclear TDP-43, exon skipping ("skiptic exons"). This diversity supports the concept in which alternative CE elements, or other TDP-43 regulated RNAs, can be incorporated into the same sensor backbone and tuned for specific biological scenarios (cell type, specific stress responses, etc...). Consistent with this, the recently described TDP-REG system (Wilkins et al., 2024) designed and AI-generated de novo CE sequences to express reporters or gene payloads, and screened multiple candidates to identify the appropriate RNA elements required for this response. These findings demonstrate that CE sequences beyond UNC13A can serve as robust TDP-43 sensing elements when optimized. Our results complement this work by demonstrating that CUTS achieves tight baseline control and a steep dynamic range (>110,000-fold induction over baseline in HEK293 cells), while maintaining compatibility across both non-neuronal and neuronal model systems, as shown in the revised manuscript.

In the revised manuscript, we show direct comparisons indicating that CUTS outperforms single-CE sensors such as UNC13A-TS and CFTR-TS under identical conditions. This supports independent work from other groups that alternative CE sequences can be engineered into effective sensors, depending on their paradigm and model systems. We have clarified this in the revised Discussion and now note that CUTS is adaptable to alternative CE inserts.

> *(3) Could the authors provide evidence of the utility of their biosensor in disease relevant systems that do not rely on TDP-43 KD? For example, does this biosensor report on TDP-43 loss of function in C9orf72 iPSNs in a time-dependent manner? Alternatively, groups have modeled TDP-43 proteinopathy in wildtype iPSNs via MG132 treatment.*

We thank the reviewer for this important suggestion. We agree that demonstrating CUTS responsiveness in disease-relevant models independent of artificial TDP-43 knockdown would further strengthen its translational relevance. In the current study, our primary objective was to establish the sensitivity, dynamic range, and autoregulatory properties of the CUTS circuit under controlled perturbation of TDP-43 levels. siRNA-mediated depletion provides a reliable approach to establish the relationship between graded TDP-43 LOF and the CUTS sensor sensitivity/specificity. That said, CUTS is designed to detect functional TDP-43 loss irrespective of the upstream cause. As the reviewer notes, disease-relevant systems, such as C9orf72 iPSC-derived neurons and proteotoxic stress paradigms (e.g., MG132-induced impairment of TDP-43 nuclear function), are important for future studies. We are currently evaluating CUTS in iPSC-derived neuronal models of TDP-43 proteinopathy, but are optimizing the induction system, promoters, and timing. It should be noted that C9orf72 iPSC neurons do not exhibit TDP-43 LOF using standard differentiation protocols. Regarding pharmacological stress, we have shown that acute sodium arsenite treatment can activate CUTS (Figure 3). In a concurrent study under revision, we show that MG132 similarly causes TDP-43 LOF and CUTS activation (Xie et al., 2025). Notably, none of these induce complete nuclear loss of TDP-43; instead, they show nuclear TDP-43 retention or modest mislocalization. This suggests that TDP-43 LOF may also result from nuclear redistribution and dysfunction under these stress conditions, rather than from complete nuclear loss. We look forward to presenting these ongoing studies in the future.

References

Brown A-L, Wilkins OG, Keuss MJ, Kargbo-Hill SE, Zanovello M, Lee WC, Bampton A, Lee FCY, Masino L, Qi YA, Bryce-Smith S, Gatt A, Hallegger M, Fagegaltier D, Phatnani H, NYGC ALS Consortium, Newcombe J, Gustavsson EK, Seddighi S, Reyes JF, Coon SL, Ramos D, Schiavo G, Fisher EMC, Raj T, Secrier M, Lashley T, Ule J, Buratti E, Humphrey J, Ward ME, Fratta P. 2022. TDP-43 loss and ALS-risk SNPs drive mis-splicing and depletion of UNC13A. Nature 603:131–137. doi:10.1038/s41586-022-04436-3

Cohen TJ, Hwang AW, Restrepo CR, Yuan C-X, Trojanowski JQ, Lee VMY. 2015. An acetylation switch controls TDP-43 function and aggregation propensity. Nat Commun 6:5845. doi:10.1038/ncomms6845

Huang W-P, Ellis BCS, Hodgson RE, Sanchez Avila A, Kumar V, Rayment J, Moll T, Shelkovnikova TA. 2024. Stress-induced TDP-43 nuclear condensation causes splicing loss of function and STMN2 depletion. Cell Rep 43:114421. doi:10.1016/j.celrep.2024.114421

Keating SS, Bademosi AT, San Gil R, Walker AK. 2023. Aggregation-prone TDP-43 sequesters and drives pathological transitions of free nuclear TDP-43. Cell Mol Life Sci 80:95. doi:10.1007/s00018-023-04739-2

Mann JR, Gleixner AM, Mauna JC, Gomes E, DeChellis-Marks MR, Needham PG, Copley KE, Hurtle B, Portz B, Pyles NJ, Guo L, Calder CB, Wills ZP, Pandey UB, Kofler JK, Brodsky JL, Thathiah A, Shorter J, Donnelly CJ. 2019. RNA Binding Antagonizes Neurotoxic Phase Transitions of TDP-43. Neuron 102:321-338.e8. doi:10.1016/j.neuron.2019.01.048

Wilkins OG, Chien MZYJ, Wlaschin JJ, Barattucci S, Harley P, Mattedi F, Mehta PR, Pisliakova M, Ryadnov E, Keuss MJ, Thompson D, Digby H, Knez L, Simkin RL, Diaz JA, Zanovello M, Brown A-L, Darbey A, Karda R, Fisher EMC, Cunningham TJ, Le Pichon CE, Ule J, Fratta P. 2024. Creation of de novo cryptic splicing for ALS and FTD precision medicine. Science 386:61–69. doi:10.1126/science.adk2539

Xie L, Zhu Y, Hurtle BT, Wright M, Robinson JL, Mauna JC, Brown EE, Ngo M, Bergmann CA, Xu J, Merjane J, Gleixner AM, Grigorean G, Liu F, Rossoll W, Lee EB, Kiskinis E, Chikina M,

Donnelly CJ. 2025. Contextdependent Interactors Regulate TDP-43 Dysfunction in ALS/FTLD. BioRxiv. doi:10.1101/2025.04.07.646890

Yu H, Lu S, Gasior K, Singh D, Vazquez-Sanchez S, Tapia O, Toprani D, Beccari MS, Yates JR, Da Cruz S, Newby JM, Lafarga M, Gladfelter AS, Villa E, Cleveland DW. 2021. HSP70 chaperones RNA-free TDP-43 into anisotropic intranuclear liquid spherical shells. Science 371. doi:10.1126/science.abb4309.

https://doi.org/10.7554/eLife.101216.2.sa0